Hindawi
Advances in High Energy Physics
Volume 2022, Article ID 9735729, 20 pages
https://doi.org/10.1155/2022/9735729

Research Article

Probing Triple Higgs Self-Coupling and Effect of Beam Polarization in Lepton Colliders

Ijaz Ahmed,[1] **Ujala Nawaz**,[1] **Taimoor Khurshid**,[2] **and Shamona Fawad Qazi**[3]

[1]*Riphah International University, Sector I-14, Hajj Complex, Islamabad, Pakistan*
[2]*International Islamic University, H-10 Islamabad, Pakistan*
[3]*Quaid-i-Azam University, Islamabad, Pakistan*

Correspondence should be addressed to Ijaz Ahmed; ijahmed75@gmail.com

Received 26 October 2021; Revised 23 March 2022; Accepted 18 May 2022; Published 6 July 2022

Academic Editor: Theocharis Kosmas

One of the main objectives of almost all future (lepton) colliders is to measure the self-coupling of triple Higgs in the Standard Model. By elongating the Standard Model's scalar sector, using incipient Higgs doublet along with a quadratic (Higgs) potential can reveal many incipient features of the model and the possibility of the emergence of additional Higgs self-couplings. The self-coupling of the Higgs boson helps in reconstructing the scalar potential. The main objective of this paper is to extract Higgs self-coupling by numerically analyzing several scattering processes governed by two Higgs doublet models (2HDM). These scattering processes include various possible combinations of final states in the triple Higgs sector. The determination of production cross-section of scattering processes is carried out using two different scenarios, one with and other without polarization of incoming beam, and is extended to a center of mass energy up to $\sqrt{s} = 3\text{TeV}$. The computation is carried out in type-1 2HDM. Here, we consider the case of exact alignment limit ($s_{\beta\alpha}$=1) and masses of extra Higgs states are equal, that is, $m_H = m_{H^0} = m_{A^0} = m_{H^\pm}$. This choice minimizes the oblique parameters. The decays of the final state of each process are investigated to estimate the number of events at an integrated luminosity of 1 ab^{-1} and 3 ab^{-1}.

1. Introduction

It is the Higgs mechanism that explains the origin of mass for elementary particles in Standard Model (SM) via an electroweakly broken symmetry mechanism. After the discovery of the most awaited Higgs particle at a mass of 125 GeV, by CMS and ATLAS experiments, one of the major aims of the Large Hadron Collider (LHC) [1, 2] is to study the properties of this particle such as precision measurement of its mass, production rate, coupling to SM particles, and spin-parity. These studies indicate that the discovered particle is in good agreement with the SM predictions. The Higgs sector could be more complicated for what is understood as yet and Beyond the Standard Model (BSM) effects could appear from exact measurements of the couplings with fermions and bosons, which can be determined from the Higgs boson production processes and decays. Two Higgs doublet model (2HDM) is one of the simplest extensions of the Standard Model. A second complex doublet SU(2) is added into the SM and forms the 2HDM; as a result, we get five Higgs states, one CP-odd scalar (A^0), two CP even scalars (H^0, h^0), and two charged Higgs bosons (H^+, H^-).

LHC is the biggest particle accelerator, where two beams of protons collide with each other and the resulting collision events are recorded. These events give us information about the beginning of the universe and properties of particles which make up the universe. Hadron colliders are discovery machines as they can reach the highest possible beam energies and, therefore, are powerful probes to new energy ranges. For examining the Higgs particles and their properties, a lepton collider is necessary, as these are the natural precision machines. In a lepton collider, the initial state of each event is known accurately and high precision of measurements can be achieved. The Future Circular Collider

(FCC-ee) [3] at CERN, the Circular Electron-positron Collider (CEPC) [4] in China, and the International Linear Collider (ILC) [5] are designed to produce many Higgs bosons and investigate their properties.

A very precise computation of Higgs self-coupling and the production cross-section of double Higgs process can be an important probe for this cosmological scenario. The cross-sectional values of double Higgs production in SM are insignificant, but Higgs self-coupling measurement required by new physics is quite challenging and enhanced by sizeable factors. Because of the presence of multijet final states, the measurement places many challenges on detector technologies and event reconstruction techniques. Hence, it is challenging to investigate the possibilities of measuring the Higgs self-coupling at particle colliders. Several experiments were carried out at LHC, and they provide beneficial results. But in reality, a more precise machine like a lepton collider is always required for the thorough study of Higgs particle and its properties with high precision, where the initial state is well defined in a lepton collider. One can easily find the four momenta from the products which helps in reconstructing the event.

The precise measurement of Higgs self-coupling gives information about the electroweak symmetry breaking (EWSB) mechanism as well as understanding of the scalar potential of Higgs field. The process $e^+e^- \longrightarrow ZHH$, also known as Higgs-strahlung is best suited to measure the trilinear Higgs self-coupling in SM. Such an effort was made earlier also where trilinear Higgs couplings in relation to various Higgs bosons pairs connected to Z boson were examined [6]. Some of the double and triple Higgs boson couplings were also examined [7, 8]. The trilinear and quartic Higgs coupling have been studied in the past within MSSM [9].

The triple Higgs production has been studied in the context of linear colliders in different reports. The radiative corrections to the triple Higgs coupling have been studied in [10]. Similarly, the production cross-section of triple Higgs production at e^+e^- collisions has been studied in Ref. [7, 11], where they analyze different sets of the Higgs boson masses and evaluate the cross-section of different processes which involve three Higgs bosons as a function of the center of mass energy of a linear collider. The ratio of triple Higgs coupling in 2HDM to that in SM has been studied in detail in Ref. [12] taking into account the perturbativity requirements, vacuum stability, and Higgs boson mass limits from direct and indirect searches. The effect of triple Higgs coupling in the production of Higgs pairs in 2HDM has been discussed in Ref. [13] for different set of center of mass energies and integrated luminosities of a linear e^+e^- collider. A similar study has also been performed in MSSM in Ref. [14]. A different work reports the effect of quantum corrections and triple Higgs self-interactions in the neutral Higgs pair production in 2HDM in Ref. [15]. In addition, triple Higgs couplings are also measured and discussed in detail in 2HDM type 1 and type 2 at High Luminosity LHC (HL-LHC) [16, 17] will be soon in operation.

The role of positron polarization at future e^+e^- colliders has been reviewed in great detail in the past [18] and updated for the case of 30% positron polarization [19]. These reports identified three main benefits of positron polarization. In this report, we will trace the influence of these through the physics topics of the 250 GeV stage of the ILC. There are three main effects of positron beam polarization which will be discussed in the context of specific physics examples in this note:

(i) Positron polarization allows us to obtain subsamples of the data with higher rates for interesting physics processes and lower rates for backgrounds. Since sensitivities do not combine as a linear sum, the combination of results from, e.g., two data sets with small and large signal-to-background ratio, respectively, is more sensitive than a single data set with the same total number of signal and background events

(ii) Positron polarization offers four distinct data sets instead of the two available if only the electron beam can be polarized. Most important reactions can be studied with the opposite-sign polarization modes only, but there are measurements in which the two like-sign polarization states give additional or even unique information. The flexibility in choosing between these configurations (and possibly even five more when considering parts of the data to be taken with zero longitudinal polarization) is a unique asset of the ILC

(iii) The likely most important effect is the control of systematic uncertainties

In our study, several scattering processes and their possible Higgs self-couplings are determined. The production cross-section as a function of the center of mass-energy and polarization of incoming beam is calculated. The results are obtained within the framework of 2HDM taking into consideration the theoretical and experimental constraints.

2. Two Higgs Doublet Model 2HDM

The simplest extension to SM is 2HDM with a different Higgs field but based on an identical gauge field with the same fermion content. The 2HDM consists of 2 Higgs isospin doublets containing hypercharge content of original Higgs field, with 8 degrees of freedom.

$$\phi_1 = \begin{pmatrix} \phi_1^+ \\ \phi_1^0 \end{pmatrix}, \phi_2 = \begin{pmatrix} \phi_2^+ \\ \phi_2^0 \end{pmatrix}. \quad (1)$$

When symmetry is spontaneously broken, in addition to three gauge bosons, the $W^\pm$ and Z^0, we get five new physical Higgs bosons: the two CP-even neutrals h and H, one CP-odd neutral A, and two charged scalars $H^\pm$.

When a discrete Z_2 symmetry is applied on the Lagrangian, it results in four possible types of 2HDM which satisfy the GWP [20] criterion.

In type-1, both quarks and leptons couple to ϕ_2 while in type-2, up type quarks couple to ϕ_2, whereas down type quarks and charged leptons couple to ϕ_1. Similarly, in

type-3, up type quarks and charged leptons couple to ϕ_2 while down type quarks couple to ϕ_1. This type is sometimes called flipped. In type-4, all charged leptons couple to ϕ_1 while all quarks couple to ϕ_2. This type is also called lepton specific.

2.1. Softly Broken Z_2 Symmetry. A discrete Z_2 symmetry is applied on the Lagrangian which constrains it. The Higgs basis is defined as

$$\phi_1 = \begin{pmatrix} G^+ \\ \frac{1}{\sqrt{2}}\left[v + S_1 + \iota G^0\right] \end{pmatrix}, \phi_2 = \begin{pmatrix} H^+ \\ \frac{1}{\sqrt{2}}\left[S_2 + \iota S_3\right] \end{pmatrix}, \quad (2)$$

where $(\iota = 1, 2)$ and $v = \sqrt{v_1^2 + v_2^2}$. G^0, S_1, S_2, and S_3 are hermitian Klein-Gordon fields while G^+ and H^+ are complex Klein-Gordon fields.

Invoking a Z_2 symmetry removes flavor-changing neutrals current (FCNCs) at tree level. In the Higgs basis, the scalar potential is then written as

$$V(\phi_1, \phi_2) = m_1^2|\phi_1|^2 + m_2^2|\phi_2|^2 - \left[m_3^2\phi_1^+\phi_2 + h.c.\right] + \frac{\Lambda_1}{2}\left|(\phi_1^+\phi_1)^2 + \frac{\Lambda_2}{2}(\phi_2^+\phi_2)^2 + \Lambda_3|\phi_1|^2|\phi_2|^2 + \Lambda_4|\phi_1^+\phi_2|\right|^2, \quad (3)$$

$$+\left[\frac{\Lambda_5}{2}(\phi_1^+\phi_1)^2 + h.c.\right] + \left[(\Lambda_6\phi_1^+\phi_1 + \Lambda_7\phi_2^+\phi_2)\phi_1^+\phi_2 + h.c.\right]. \quad (4)$$

The coupling constant m_1^2, m_2^2, Λ_1, Λ_2, Λ_3, and Λ_4 are real whereas m_3^2, Λ_5, Λ_6, and Λ_7 are complex parameters but for simplification they are also taken as real. The scalar potential can be decomposed as a sum of quadratic, cubic, and quartic interactions. The quadratic terms define the physical Higgs states and their masses. Diagonalization of quadratic mass terms gives masses of all extra Higgs bosons [21]. The sin $(\beta - \alpha)$ is the mixing angle among the CP-even Higgs states and is also denoted by $s_{\beta\alpha}$.

The exact alignment limit, i.e., $s_{\beta\alpha} = 1$ is considered, so that h^0 becomes indistinguishable from the Standard Model Higgs boson with respect to coupling and mass. Hence, there are only six independent parameters of the model which are important for our study, which include m_h, m_{H^0}, and m_{A^0}, the ratio of vacuum expectation value tan β, $s_{\beta\alpha}$, and ${m_3}^2$. The parameter ${m_3}^2$ indicates how is the discrete symmetry broken [22]. In Equation (4), the cubic and quartic terms define the interactions and couplings between the new states in 2HDM.

2.2. Theoretical and Experimental Constraints. The parameters of scalar potential in 2HDM are reduced both by the theoretical developments, as well as results of experimental searches. The theoretical constraints to which 2HDM is subjected comprise of vacuum stability, unitarity, and perturbativity.

(i) *Stability*. Requirement of a stable vacuum keeps the potential bounded from below. The potential must be positive at large values of fields for any direction in the plane [23, 24]

(ii) *Unitarity*. Unitarity constraints do not allow the scattering amplitudes to have probability more than unity. The amplitude needs to be flat at asymptotically large values of energy [25, 26]

(iii) *Perturbitivity*. The potential needs to be perturbative to fulfill the requirement that all quartic couplings of scalar potential obey $\Lambda_i \leq 8\pi$ for all i

The parameters are tested as if they obey the abovementioned theoretical constraints which are checked by 2HDMC [27]. The 2HDM parameters are also constrained by recent experimental searches by integrating the latest versions of HiggsBounds [28] and HiggsSignals [29] with 2HDMC libraries. According to a study carried out in reference [30], the flavor physics limits are presented, and Figure 1 particularly provides available parameter space which is not yet excluded. The charged Higgs $H^\pm$ present in 2HDM, which is comparable to SM, also makes a novel contribution in flavor limits. Masses of all extra Higgs bosons are set to be equal, that is, $m_H = m_{H^0} = m_{A^0} = m_{H^\pm}$. This choice minimizes the oblique parameters, and all the electroweak observables are close to SM. The decay of H^0 to vector boson pair is suppressed in the exact alignment limit. According to [26] in type-1, the neutral meson mixing and results of $B_s^0 \longrightarrow \mu^+\mu^-$ restrict the low tan β. The analysis is, therefore, carried out in the range $2 < \tan\beta < 40$. The region in which theoretical constraints are obeyed by ${m_3}^2$ is shown in Figure 2. The range of values of m_{12}^2 for different tanβ are extracted by applying theoretical constraints on each point to get the selected range of these values. Both selected values are plotted together in 1. So by varying the masses of all Higgs combinely in the exact alignment limit of sin $(\alpha - \beta) = 1$ and selected values of tan β and m_{12}^2 from 1, the allowed masses are obtained by applying the theoretical constraints in 2HDMC as shown in Table 1.

2.3. Higgs Self-Couplings in 2HDM. In 2HDM, Higgs self-couplings as a function of Λ_i are given by Equations (5) to (10). The values for two independent parameters are selected to be $s_{\beta\alpha} = 1$ and $c_{\beta\alpha} = 0$. Due to exact alignment limit and equal masses of all extra Higgs bosons, three other parameters Λ_4, Λ_5, and Λ_6 also vanish. Among all the Higgs self-couplings, only the one given by g_{hhH} vanishes. However the couplings g_{hHH} and g_{hAA} are equal to each other and $g_{HHH}/g_{HAA} = 3$. These predictions can also be checked experimentally. If $\Lambda_{345} = \Lambda_3 + \Lambda_4 + \Lambda_5$, then, we can write

$$g_{h^0h^0h^0} = -3\iota v\left(\left(\Lambda_7 c_{\beta\alpha}^2 + 3\Lambda_6 s_{\beta\alpha}^2\right)c_{\beta\alpha} + \left(\Lambda_{345}c_{\beta\alpha}^2 + \Lambda_1\delta_{\beta\alpha}^2\right)s_{\beta\alpha}\right)_{c\beta\alpha\longrightarrow 0} - 3\iota v\Lambda_1 S, \quad (5)$$

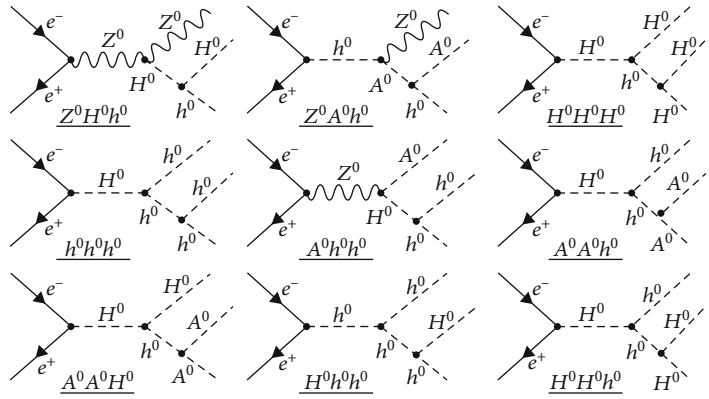

Figure 1: The Feynman diagram of various processes in 2HDM. Their amplitude shows that their cross-section is less than 10^{-11} pb, so their self coupling can be neglected.

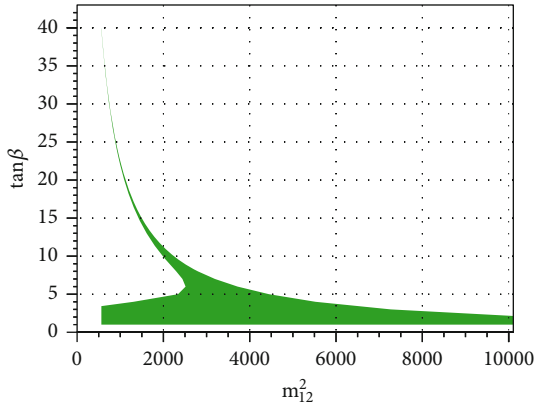

Figure 2: The plot between soft symmetry breaking term versus tan β. The region under bounded curves shows the theoretical constraints obeyed.

Table 1: The range of independent parameters calculated within type-1 2HDM.

Benchmark	Yukawa type	m_h [GeV]	$m_H = m_A = m_H^+$ [GeV]	$s_{\beta\alpha}$	t_β
1	Type-I	125	175	1	2 - 40

$$g_{h^0h^0H^0} = -\iota v\Big(\Big(\Lambda_{345}\Big(1-3s^2_{\beta\alpha}\Big)+3\Lambda_1 s^2_{\beta\alpha}\Big)c_{\beta\alpha} + 3\Big(\Lambda_6\Big(2-3s^2_{\beta\alpha}\Big)-\Lambda_7 c^2_{\beta\alpha}\Big)s_{\beta\alpha}\Big)_{c\beta\alpha\longrightarrow 0} 0, \tag{6}$$

$$g_{h^0H^0H^0} = -\iota v\Big(\Big(3\Lambda_1 c^2_{\beta\alpha}+\Lambda_{345}\Big(3s^2_{\beta\alpha}-2\Big)\Big)s_{\beta\alpha} + 3\Big(\Lambda_6+\Lambda_7\%s^2_{\beta\alpha}-3\Lambda_6 s^2_{\beta\alpha}\Big)c_{\beta\alpha}\Big)_{c\beta\alpha\longrightarrow 0} - \iota v\Lambda_3, \tag{7}$$

$$g_{h^0A^0A^0} = -\iota v\big(\Lambda_7 c_{\beta\alpha}+(\Lambda_3+\Lambda_4-\Lambda_5)s_{\beta\alpha}\big)_{c\beta\alpha\longrightarrow 0} - \iota v\Lambda_3, \tag{8}$$

$$g_{H^0H^0H^0} = -3\iota v\Big(\Big(\Lambda_1 c^2_{\beta\alpha}+\Lambda_{345}s^2_{\beta\alpha}\Big)c_{\beta\alpha} - \Lambda_7 s^2_{\beta\alpha}-3\Lambda_6 c^2_{\beta\alpha}\Big)s_{\beta\alpha}{}_{c\beta\alpha\longrightarrow 0} 3\iota v\Lambda_7, \tag{9}$$

$$g_{H^0A^0A^0} = -\iota v\big((\Lambda_3+\Lambda_4-\Lambda_5)c_{\beta\alpha}-\Lambda_7 s_{\beta\alpha}\big)_{c\beta\alpha\longrightarrow 0} \iota v\Lambda_7. \tag{10}$$

3. Triple Higgs Self-Coupling and Production Cross-Section

It is normally believed that ILC will perform efficiently in precision measurements as compared to LHC, due to its clean environment, fixed center-of-mass energy, and attainability of polarized beam. This fact emphasizes the importance of ILC for Higgs sector in terms of calculations of different scattering processes, their self-couplings, branching ratios, and estimation of number of events.

3.1. Measurement of Higgs Self-Coupling. The trilinear self-coupling can be measured directly or indirectly by using the Higgs-boson-pair production cross section or through the measurement of single-Higgs-boson production and decay modes, respectively. In fact, the Higgs-decay partial widths and the cross sections of the main single-Higgs production processes depend on the Higgs-boson self-coupling via weak loops, at next-to-leading order in electroweak interaction. Let us consider the scattering process $e^-e^+ \longrightarrow Zhh$ to study the trilinear coupling of the Higgs boson. In SM, the tree level Feynman diagrams of this process are shown in Figure 3. The left figure contains the three Higgs self-coupling vertex g_{hhh} and makes the dominant contribution in calculation of scattering amplitude. In the SM, we obtain $m_H = \sqrt{2\lambda v}$ as the simple relationship between the Higgs boson mass m_H and the self-coupling, where $v = 246$ GeV is the vacuum expectation value of the Higgs boson. The triple vertex of the Higgs field H is given by Eq. (5), and a measurement of g_{hhh} in the SM can determine m_H. An accurate test of this relationship may reveal the extended nature of the Higgs sector. The measurement of the triple Higgs boson coupling is one of the most important goals of Higgs

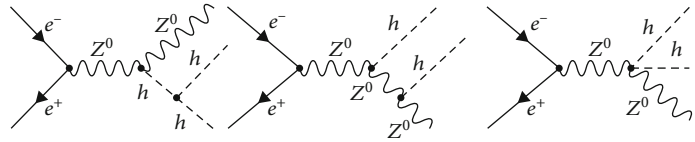

Figure 3: The left-most diagram contains the Higgs self-coupling vertex corresponding to the process $e^+e^- \longrightarrow Zhh$.

physics in a future e^+e^- linear collider experiment. This would provide the first direct information on the Higgs potential responsible for electroweak symmetry breaking. The triple Higgs boson self-coupling can be measured directly in pair production of Higgs particles at hadron and high-energy e^+e^- linear colliders. Several mechanisms that are sensitive to g_{hhh} can be exploited for this task. Higgs pairs can be produced through double Higgs-strahlung of W or Z bosons [31–43], W^+W^- or ZZ fusion [44–47]; moreover, through gluon-gluon fusion in pp collisions [48–51] and high-energy $\gamma\gamma$ fusion [52] at photon colliders.

The measurement of Higgs self-coupling within 2HDM is difficult due to the presence of more than one Higgs. The couplings in which h^0, H^0, and A^0 are intermediated and do not make a noticeable contribution because of their absolute value, which is less than 10^{-6}, so they can be neglected. Significant contributions are found to be from Z^0 coupling only, that is why only those Feynman diagrams are taken into account in which Z boson is intermediated. The scattering processes with various combinations of trilinear Higgs self-couplings need to be considered, i.e., ZHh, ZAh, HHH, hhh, Ahh, AAh, AAH, Hhh, and Hhh are shown in Feynman diagrams Figure 1 of possible processes. Their cross-section is less than 10^{-11} pb; therefore it is not possible to detect them and can be easily neglected.

To calculate the Higgs self-coupling in two Higgs doublet model, we use the scattering processes shown in Table 2. These scattering processes are the only ones which can give the cross-section greater than attobarn. In Equation (6), $g_{h^0h^0H^0}$ approaches zero so this coupling vanishes. The cross-section of scattering process $e^-e^+ \longrightarrow ZAA$ makes it possible to determine the coupling $g_{h^0A^0A^0}$. The coupling $g_{h^0H^0H^0}$ can be determined by measuring the cross-section of process $e^-e^+ \longrightarrow ZHH$. The cross-section of $e^-e^+ \longrightarrow Zh$ h extracts the coupling $g_{h^0h^0h^0}$ which could be the same as determined in SM. The coupling $g_{H^0A^0A^0}$ can be determined by two processes, $e^-e^+ \longrightarrow AHh$ and $e^-e^+ \longrightarrow AHH$, whereas the last mentioned process can also give $g_{H^0H^0H^0}$.

4. Production Cross-Section Using Polarized e^- e^+ Beams

The longitudinally polarized beams cross-section in an e^-e^+ collider can be expressed as

$$\sigma_{P_{e^-},P_{e^+}} = \frac{1}{4}\{(1+P_{e^-})(1+P_{e^+})\sigma_{RR} + (1-P_{e^-})(1-P_{e^+})\sigma_{LL} + (1+P_{e^-})(1-P_{e^+})\sigma_{RL} + (1-P_{e^-})(1+P_{e^+})\sigma_{LR}. \quad (11)$$

Table 2: The triple Higgs self-coupling contributing to scattering process while using the exact alignment limit equal to one and extra Higgs masses to be equal.

Scattering processes	Higgs self-coupling
$e^-e^+ \longrightarrow Z^0A^0A^0$	$g_{h^0A^0A^0}$
$e^-e^+ \longrightarrow Z^0H^0H^0$	$g_{h^0H^0H^0}$
$e^-e^+ \longrightarrow Z^0h^0h^0$	$g_{h^0h^0h^0}$
$e^-e^+ \longrightarrow A^0H^0h^0$	$g_{H^0A^0A^0}$
$e^-e^+ \longrightarrow A^0H^0H^0$	$g_{H^0A^0A^0}, g_{H^0H^0H^0}$

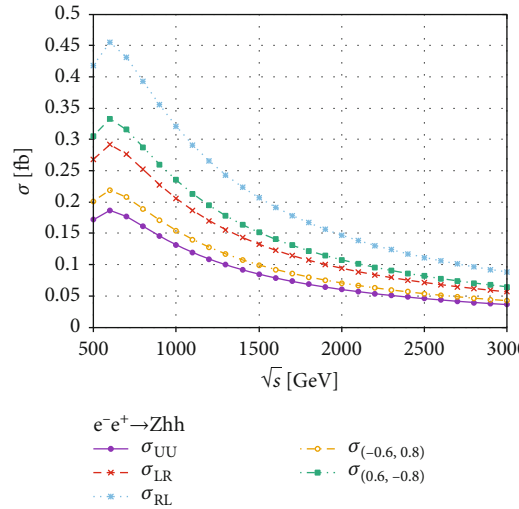

Figure 4: Total cross-section σ as a function of collider center of mass energy $\sqrt{s}$ (GeV) at Higgs masses $m_H = 150\,GeV$ or $m_H = 175\,GeV$, $\tan\beta = 10$, and $s_{\beta\alpha} = 1$ are shown.

Table 3: The cross-section in fb with unpolarized and fully polarized incoming e^-e^+ beams, where masses of extra Higgs states are fixed at $m_\phi = 150$ GeV at $\tan\beta = 5$.

	0.6 TeV $m_\phi = 150$ GeV	1 TeV $m_\phi = 150$ GeV	3 TeV $m_\phi = 150$ GeV
σ_UU	0.187 ± 0.02	0.132 ± 0.0204	0.036 ± 0.01
σ_LR	0.292 ± 0.031	0.206 ± 0.031	0.056 ± 0.02
σ_RL	0.455 ± 0.049	0.321 ± 0.050	0.082 ± 0.034
$\sigma\_((0.6,-0.8))$	0.332 ± 0.036	0.235 ± 0.036	0.065 ± 0.027
$\sigma\_((-0.6,0.8))$	0.219 ± 0.023	0.155 ± 0.02	0.045 ± 0.018

Table 4: A detailed scan of several Higgs production cross-sections in units of fb with unpolarized and fully polarized incoming e^-e^+ beams are reported. Where masses of extra Higgs states are varied over a range of $m_H = 150\,\text{GeV}$ to $m_H = 500\,\text{GeV}$.

	0.6 TeV				1 TeV				3 TeV			
	$m_\phi = 150$	$m_\phi = 175$	$m_\phi = 300$	$m_\phi = 500$	$m_\phi = 150$	$m_\phi = 175$	$m_\phi = 300$	$m_\phi = 500$	$m_\phi = 150$	$m_\phi = 175$	$m_\phi = 300$	$m_\phi = 500$
						$e^-e^+ \longrightarrow AHh$						
σ_UU	0.0059 ± 0.0012	0.0023 ± 0.0004	0.0 ± 0.0	0.0 ± 0.0	0.0078 ± 0.0023	0.0059 ± 0.0016	0.0011 ± 0.0002	0.0 ± 0.0	0.0012 ± 0.0015	0.0010 ± 0.0014	0.0005 ± 0.0004	0.0002 ± 0.0001
σ_LR	0.0091 ± 0.0019	0.0037 ± 0.0007	0.0 ± 0.0	0.0 ± 0.0	0.0121 ± 0.0035	0.0093 ± 0.0025	0.00168 ± 0.0035	0.0 ± 0.0	0.0018 ± 0.0023	0.0016 ± 0.0018	0.00092 ± 0.00059	0.0004 ± 0.0002
σ_RL	0.0143 ± 0.0029	0.0057 ± 0.0012	0.0 ± 0.0	0.0 ± 0.0	0.0189 ± 0.0056	0.0145 ± 0.0038	0.0026 ± 0.0006	0.0 ± 0.0	0.0029 ± 0.0038	0.0025 ± 0.0028	0.0014 ± 0.0009	0.00069 ± 0.0003
$\sigma\_((0.6,-0.8))$	0.0105 ± 0.0022	0.0042 ± 0.0008	0.0 ± 0.0	0.0 ± 0.0	0.0138 ± 0.0040	0.0186 ± 0.0049	0.0019 ± 0.0004	0.0 ± 0.0	0.0021 ± 0.0027	0.0018 ± 0.0021	0.0010 ± 0.0007	0.0005 ± 0.0002
$\sigma\_((-0.6,0.8))$	0.0069 ± 0.0014	0.0027 ± 0.0006	0.0 ± 0.0	0.0 ± 0.0	0.0091 ± 0.0026	0.0070 ± 0.0018	0.0012 ± 0.0002	0.0 ± 0.0	0.0014 ± 0.0018	0.0012 ± 0.0014	0.0007 ± 0.0004	0.0003 ± 0.0001
						$e^-e^+ \longrightarrow AHH$						
σ_UU	0.0018 ± 0.0004	0.0002 ± 0.00004	0.0 ± 0.0	0.0 ± 0.0	0.0042 ± 0.0013	0.0023 ± 0.0006	0.000014 ± 0.000003	0.0 ± 0.0	0.0009 ± 0.0011	0.0006 ± 0.0006	0.00017 ± 0.00087	0.000033 ± 0.0000094
σ_LR	0.0029 ± 0.0006	0.00033 ± 0.00006	0.0 ± 0.0	0.0 ± 0.0	0.0065 ± 0.002	0.0035 ± 0.0009	0.00002152 ± 0.0000043	0.0 ± 0.0	0.0014 ± 0.0017	0.0010 ± 0.0009	0.00027 ± 0.00013	0.000051 ± 0.000017
σ_RL	0.0046 ± 0.0010	0.00052 ± 0.0001	0.0 ± 0.0	0.0 ± 0.0	0.010 ± 0.003	0.0055 ± 0.0015	0.000033 ± 0.0000068	0.0 ± 0.0	0.0022 ± 0.002	0.0016 ± 0.0015	0.0004 ± 0.00020	0.000082 ± 0.000023
$\sigma\_((0.6,-0.8))$	0.0038 ± 0.0008	0.0003 ± 0.0008	0.0 ± 0.0	0.0 ± 0.0	0.0074 ± 0.0023	0.0040 ± 0.001	0.000024 ± 0.0000049	0.0 ± 0.0	0.0016 ± 0.0019	0.0011 ± 0.001	0.00031 ± 0.00015	0.0000602 ± 0.000017
$\sigma\_((-0.6,0.8))$	0.0022 ± 0.0004	0.00025 ± 0.00005	0.0 ± 0.0	0.0 ± 0.0	0.0049 ± 0.0015	0.0026 ± 0.0007	0.000016 ± 0.0000033	0.0 ± 0.0	0.0010 ± 0.0012	0.00075 ± 0.0007	0.00020 ± 0.0001	0.000039 ± 0.0000112
						$e^-e^+ \longrightarrow ZHH/ZAA$						
σ_UU	0.0527 ± 0.0060	0.0278 ± 0.0030	0.0 ± 0.0	0.0 ± 0.0	0.075 ± 0.011	0.062 ± 0.009	0.0152 ± 0.00200	0.0 ± 0.0	0.031 ± 0.009	0.030 ± 0.008	0.02423 ± 0.0052	0.0158 ± 0.0029
σ_LR	0.0824 ± 0.0093	0.0436 ± 0.0049	0.0 ± 0.0	0.0 ± 0.0	0.117 ± 0.017	0.097 ± 0.04	0.0237 ± 0.0031	0.0 ± 0.0	0.049 ± 0.015	0.047 ± 0.013	0.0379 ± 0.0082	0.0247 ± 0.0045
σ_RL	0.1284 ± 0.0146	0.0679 ± 0.0075	0.0 ± 0.0	0.0 ± 0.0	0.183 ± 0.027	0.151 ± 0.022	0.0370 ± 0.0048	0.0 ± 0.0	0.077 ± 0.023	0.073 ± 0.019	0.0590 ± 0.0127	0.0386 ± 0.0071
$\sigma\_((0.6,-0.8))$	0.0941 ± 0.0106	0.0498 ± 0.0054	0.0 ± 0.0	0.0 ± 0.0	0.134 ± 0.019	0.110 ± 0.011	0.0271 ± 0.0035	0.0 ± 0.0	0.056 ± 0.016	0.054 ± 0.014	0.0432 ± 0.0094	0.0287 ± 0.0052
$\sigma\_((-0.6,0.8))$	0.0618 ± 0.0071	0.0327 ± 0.0089	0.0 ± 0.0	0.0 ± 0.0	0.088 ± 0.013	0.072 ± 0.010	0.0178 ± 0.0023	0.0 ± 0.0	0.037 ± 0.011	0.035 ± 0.0095	0.0284 ± 0.0061	0.0185 ± 0.0034

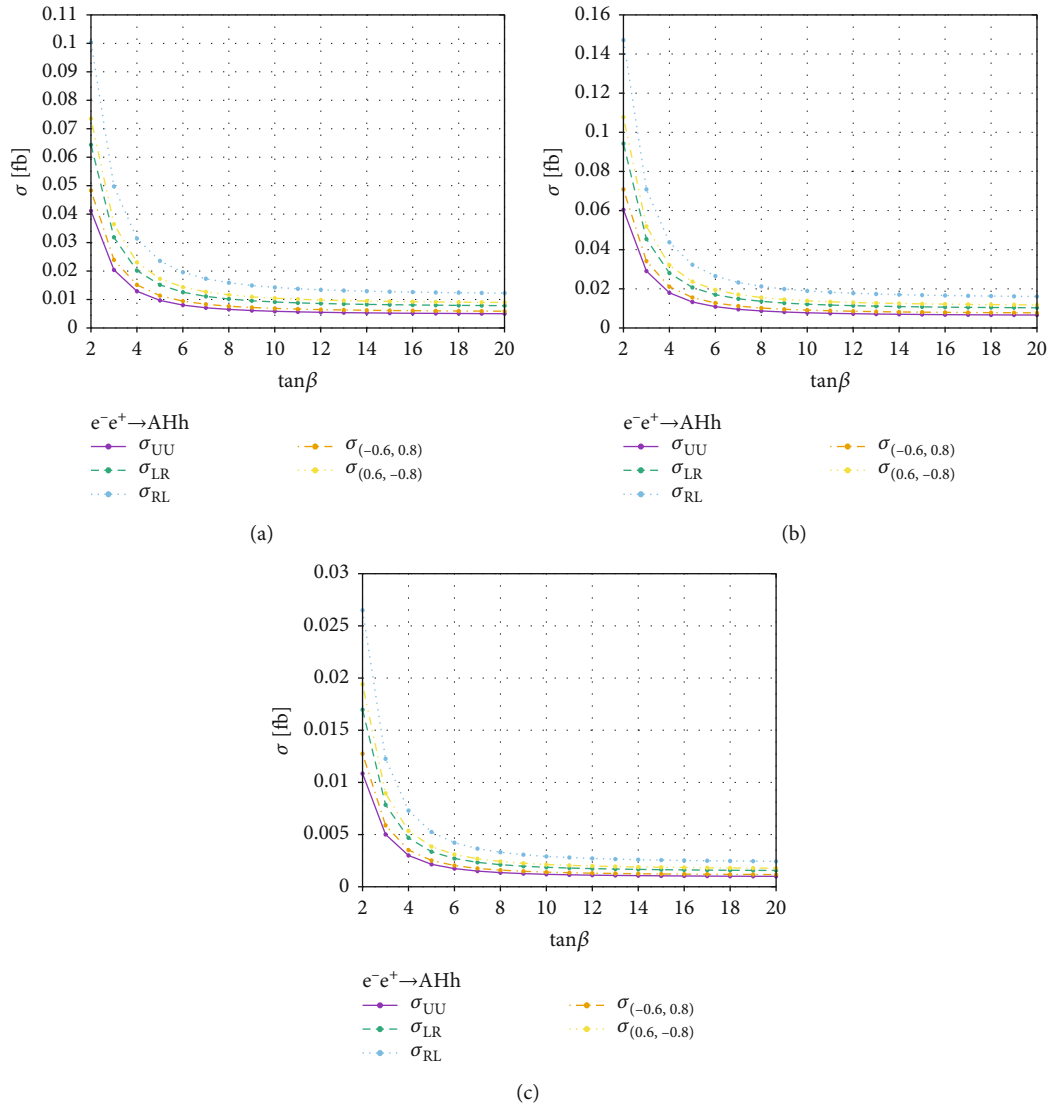

FIGURE 5: Figure shows dependency of tanβ on $\sigma(pp \longrightarrow AHh)$ at (a) $\sqrt{s} = 0.6$ TeV, (b) $\sqrt{s} = 1$ TeV, and (c) $\sqrt{s} = 3$ TeV energies.

In e^-e^+ experiments, the prominent or dominant processes are

(i) Scattering (t and u-channel), vector boson fusions

(ii) Annihilation (s-channel), higgsstrahlung process

In annihilation process of e^-e^+, helicities are coupled with the spin of particles whose interchange process occurs in direct channel. According to the SM, a vector particle resulting from annihilation carry total spin angular momentum ($J = 1$); therefore, only left-right (LR) and right-left (RL) configurations contribute in this process [53]. Higgs production in association with neutral Z boson, known as Higgsstrahlung process, is an example of annihilation process [54]. In order to study these processes, suitable combination of polarization plays an important role in suppressing the background radiations and enhancing signal rate. New searches can be performed, where rates are predicted to be very small by increasing signal/background ratio using high luminosity. On the other hand, in scattering process, the helicities of incoming beams are independent of each other and are directly connected to any resulting particle at the vertex. The helicities of e^- and e^+ can be the same, and all four spin configurations are possible in this case [53]. Vector bosons fusions that contributes to Higgs production are an example of scattering process [54]. Setting the polarization of incoming particles independently is a property that leads us towards searches of new characteristics of particles, chiral couplings, and quantum numbers with level suppositions.

5. The Production Cross-Section of Scattering Processes

For the computation of production cross-section of various scattering processes, CalcHEP_3.7.6 package [55] is used. The parameters of Standard Model are used from the [56], which are $m_e = 0.51099$ MeV, $m_Z = 91.1876$ GeV, and $s_w = 0.474$. The Higgs boson mass is taken to be $m_h = 125.09$

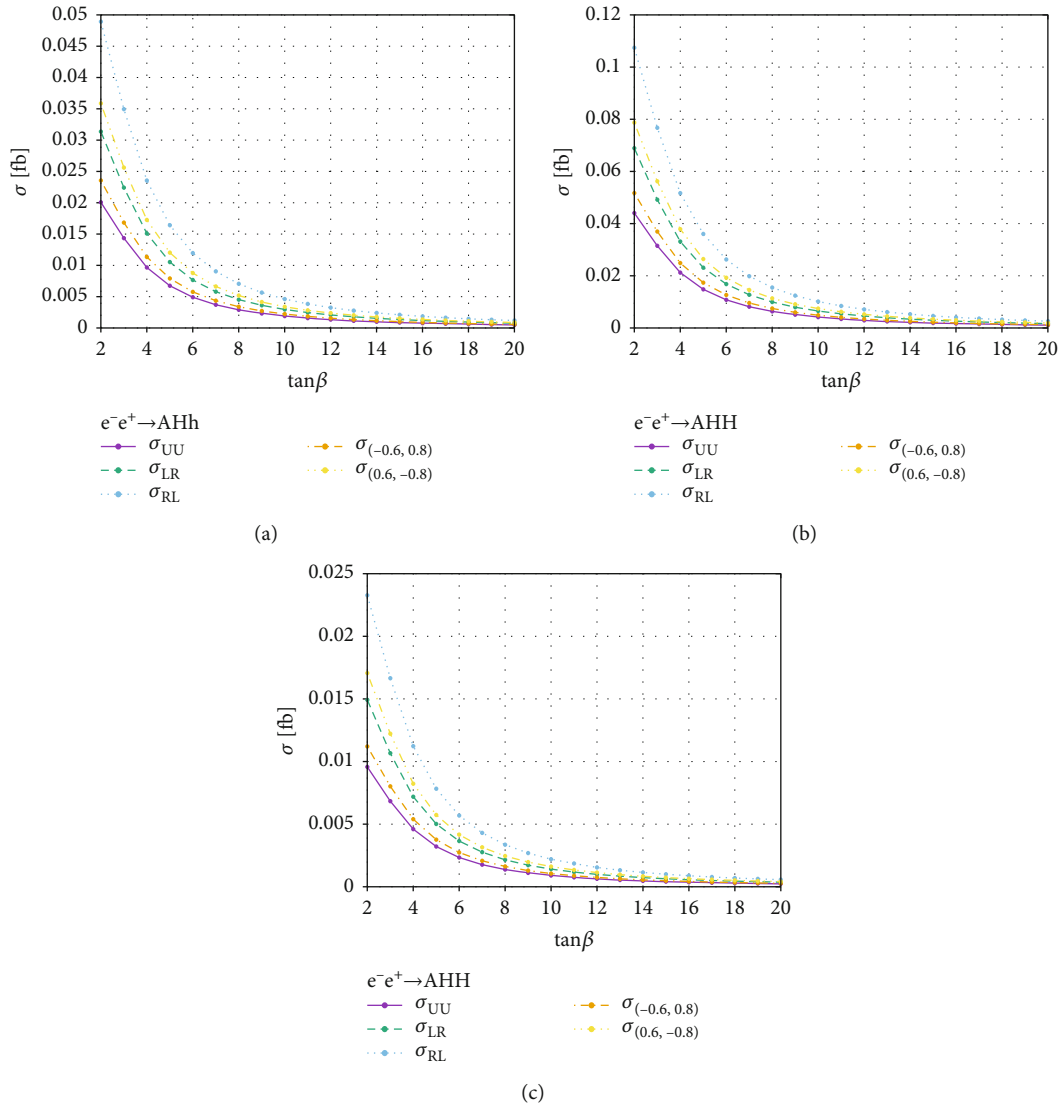

FIGURE 6: In figures, the production cross sections $\sigma(pp \longrightarrow AHH)$ are shown as a function of tanβ at (a) 0.6 TeV, (b) 1 TeV, and (c) 3 TeV energies.

GeV. The 2HDM parameters are already discussed in the previous section. The cross-sections of various scattering process are given below:

$$e^- e^+ \longrightarrow Zhh. \tag{12}$$

The cross-section of this prominent channel is shown in Figure 4. It can be seen that the maximum cross-section of the unpolarized beam is approximately 0.187 fb at 0.6 TeV and decreases for higher energies. However, the polarized beam enhances the cross-section as compared to the unpolarized beam. The right-handed electron beam and left-handed positron beam (σ_{RL}) maximize the cross-section which is around 0.455 fb at 0.6 TeV. Moreover, the distribution of left-handed electron beam and right-handed positron beam (σ_{LR}), and two cases of polarization beam $\sigma_{(0.6,-0.8)}$ and $\sigma_{(-0.6,0.8)}$ are also given in Table 3.

In Table 4, a very comprehensive scan of production cross-sections of possible processes where the triple Higgs vertex exist is performed by varying center of mass energy as well as by varying Higgs mass. Each cross-section value is estimated along with uncertainties for all possible colliding beam polarization scenarios. A significant enhancement in σ_{RL} is observed when electron beam is right handed, and positron beam is left handed specifically in AHh, ZHH, and ZAA, while moderate enhancement is observed in AHH.

In Figure 5, beam polarization effects are observed for $(e^+e^- \longrightarrow AHh)$ at three different energies, fully right handed electron, and left handed positron provides the enhancement by a factor of approximately 2.5 for tan β = 3 at $\sqrt{s} = 0.6$ TeV, $\sqrt{s} = 1$ TeV, and $\sqrt{s} = 3$ TeV energies.

Similar enhancement factor is observed for the process $(e^+e^- \longrightarrow AHH)$ in Figure 6. This enhancement factor remains independent of center of mass energy.

In Figure 7, the $\sigma(e^+e^- \longrightarrow ZAA)$ stays at constant values as a function of tan β from equation (9) as expected.

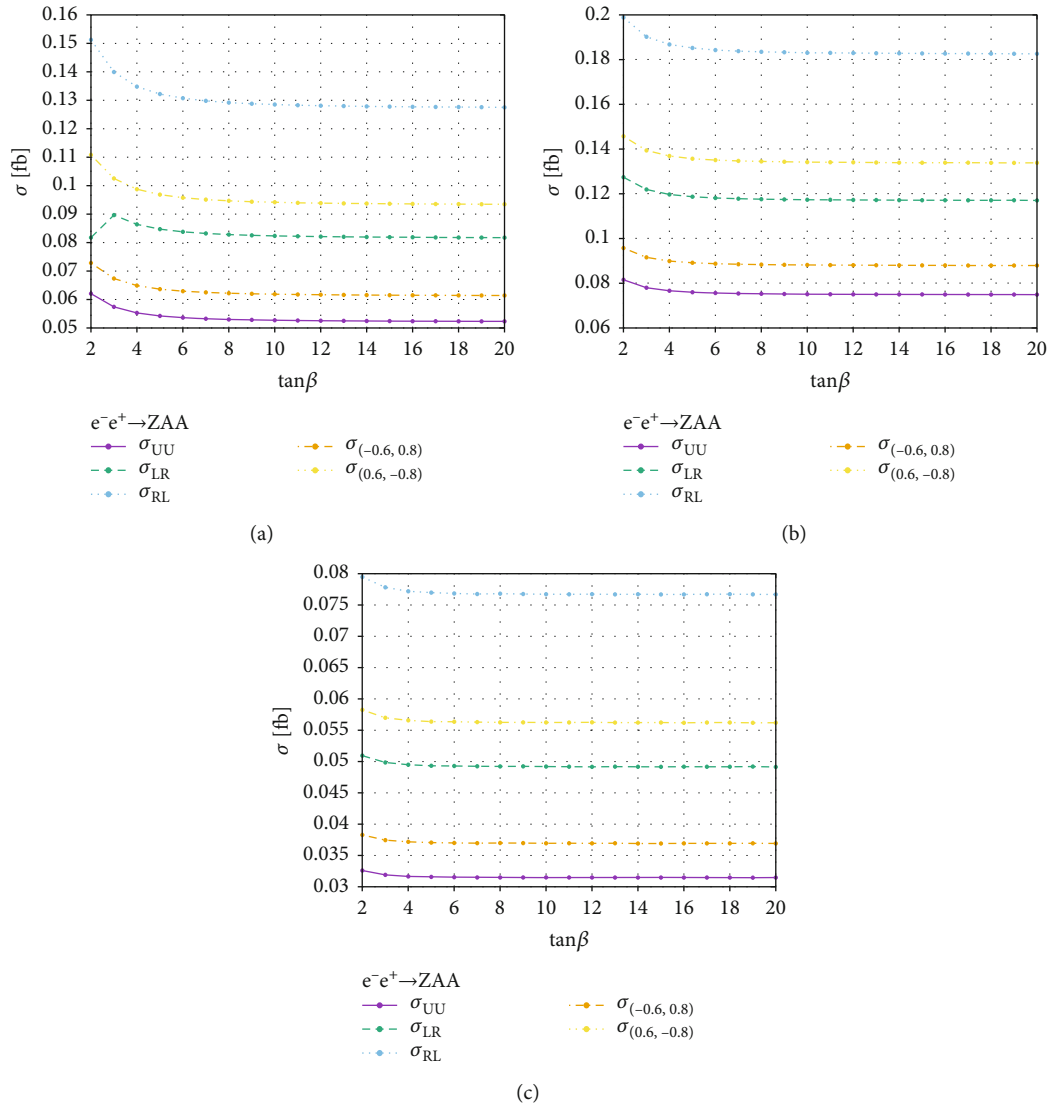

FIGURE 7: Figure (a) is plotted to discuss the behaviour of $\sigma(e^+e^- \longrightarrow ZAA)$ at $\sqrt{s} = 0.6$ TeV, whereas in (b) and (c), same variables are plotted at $\sqrt{s} = 1$ TeV and $\sqrt{s} = 3$ TeV, respectively.

The other processes $\sigma(e^+e^- \longrightarrow Zhh)$ and $\sigma(e^+e^- \longrightarrow ZHH)$ are also evaluated in Figures 8 and 9 at three different selected values of energies.

Table 5 depicts the details of production cross-section of processes containing trilinear Higgs self-coupling and dependencies on tanβ, $\sqrt{s}$, and various combinations of both colliding beam polarizations at $m_\phi = 150$ GeV. We have not observed any significant enhancement in σ_{RL} as a function of tanβ in all processes except in AHH, where a reduction in tanβ is observed. The unpolarized cross-section for Zhh is around $\sigma_{UU} = 0.1869$ fb at $\sqrt{s} = 0.6$ TeV, and it rises to 0.45 fb for fully polarized beams (σ_{RL}), then decreases slowly for higher energies, i.e., $\sigma_{RL} = 0.312$ ($\sqrt{s} = 1$ TeV) and $\sigma_{RL} = 0.089$ ($\sqrt{s} = 3$ TeV). Similarly, one can extract the σ_{RL} values for other processes from this table.

$$e^-e^+ \longrightarrow \frac{ZHH}{ZAA}. \tag{13}$$

Consider the scattering process $e^-e^+ \longrightarrow ZHH/ZAA$ for determination of cross-section distribution. Since according to Equations (7) and (8), the couplings $g_{h^0H^0H^0}$ and $g_{h^0A^0A^0}$ of both scattering processes are same, and in terms of parameter space, m_H and m_A are also identical, hence, these two scattering process $e^-e^+ \longrightarrow ZHH$ and $e^-e^+ \longrightarrow ZAA$ can be considered same. Therefore, the cross-section as a function of center of mass of energy for both becomes equal. The plots for different polarizations of beam are shown in Figure 10. The scattering amplitudes for Feynman diagrams shown in Figures 11 and 12 are same. Only those diagrams are selected in both figures where Z bosons are mediating contributing maximally in production cross-section. We consider two different fixed values of extra Higgs states, i.e., $m_H = 175$ GeV and $m_H = 150$ GeV and compare their cross-section. From Figure 10, it is clear that for $m_H = 175$ GeV the maximum cross-section of unpolarized beam is 0.062 fb at 1 TeV which decreases slowly with increase in energy. The maximum cross-section of right handed

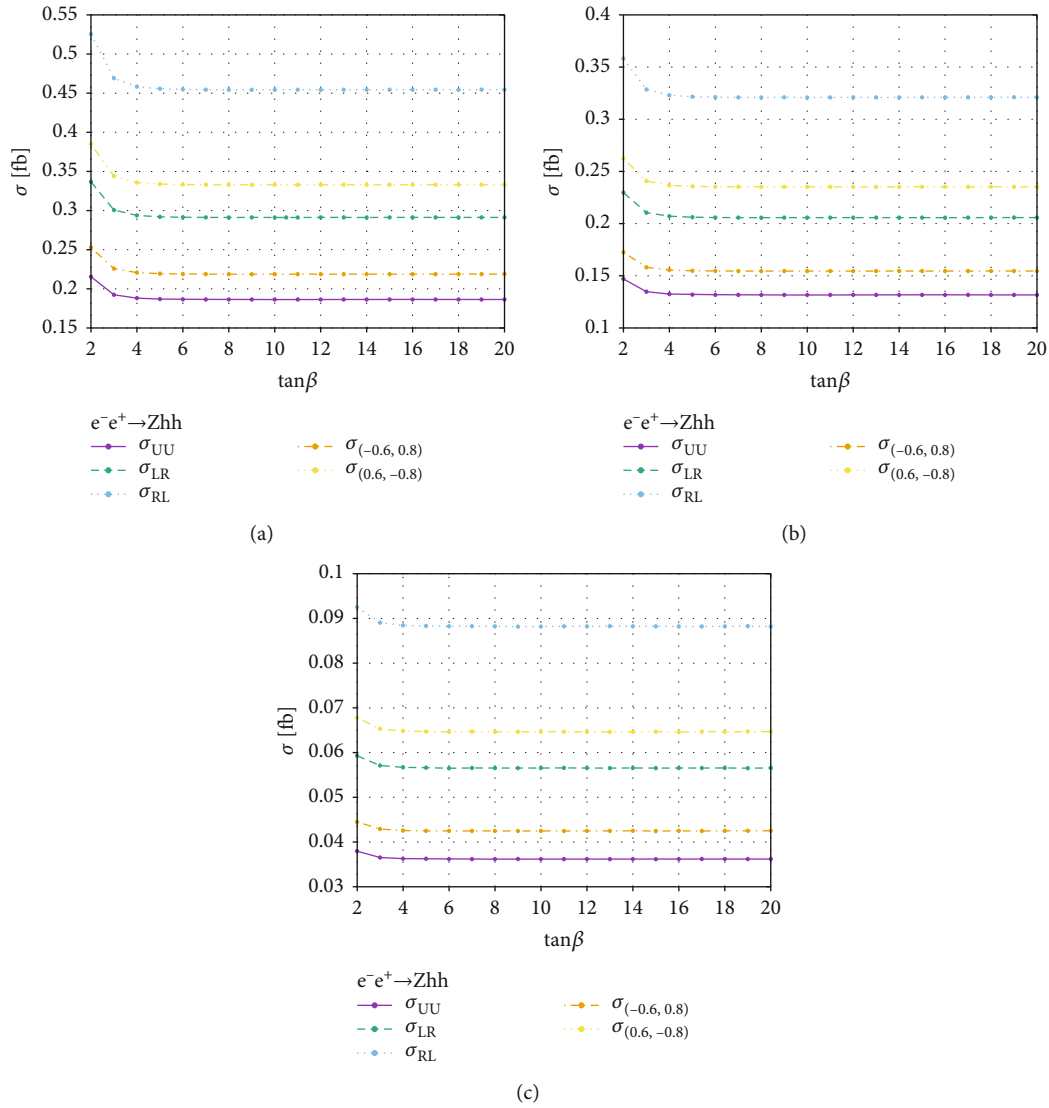

FIGURE 8: Figure shows dependency of tanβ on $\sigma(e^+e^- \longrightarrow Zhh)$ at (a) $\sqrt{s} = 0.6$ TeV, (b) $\sqrt{s} = 1$ TeV, and (c) $\sqrt{s} = 3$ TeV energies.

polarized electron and left handed polarized positron beam is around 0.151 fb. When $m_H = 150$ GeV, then, the unpolarized cross-section reaches about 0.075 fb and then decreases slowly with higher energy. Additionally $\sigma_{RL} = 0.183\, fb$, which shows that RL scenario enhances the cross-section. From comparison of two mass values, it is clear that a value of 150 GeV shows maximum cross-section as compared to 175 GeV.

$$e^- e^+ \longrightarrow AHh. \tag{14}$$

For the next scattering process $e^-e^+ \longrightarrow AHh$, the distributions are shown in Figure 13. When the mass of extra Higgs states are taken as 175 GeV; then, the cross-section of $\sigma_{UU}(\text{unpolarized}) = 0.0059\, fb$ at $\sqrt{s} = 1$ TeV. The maximum cross-section of polarized beam is $\sigma_{RL} = 0.0145\ fb$. Similarly when $m_H = m_A = m_{H^\pm} = 150\ GeV$ are used then unpolarized cross-section is 0.0078 fb and right-handed polarized electron beam and left-handed polarized positron beam (σ_{RL}) are 0.0189 fb. Coupling $g_{H^0A^0A^0}$ can be extracted from this scattering process but the cross-section is quite small. The diagrams contributing in this process are given in Figure 14, where only s-channel diagrams mediating Z bosons are considered because of having largest contribution.

$$e^- e^+ \longrightarrow AHH. \tag{15}$$

The last cross-section is calculated for the scattering process $e^-e^+ \longrightarrow AHH$. The cross-section plot is shown in Figure 15 and Figure 16 shows the Feynman diagrams for AHH production via triple Higgs vertices formed by HHH, AHH, and hHH from left to right, respectively. This process has smallest cross-section as compared to others. The unpolarized beam has a cross-section of 0.0023 fb at $\sqrt{s} = 1$TeV, where $m_H = m_A = m_{H^\pm} = 175$ GeV.

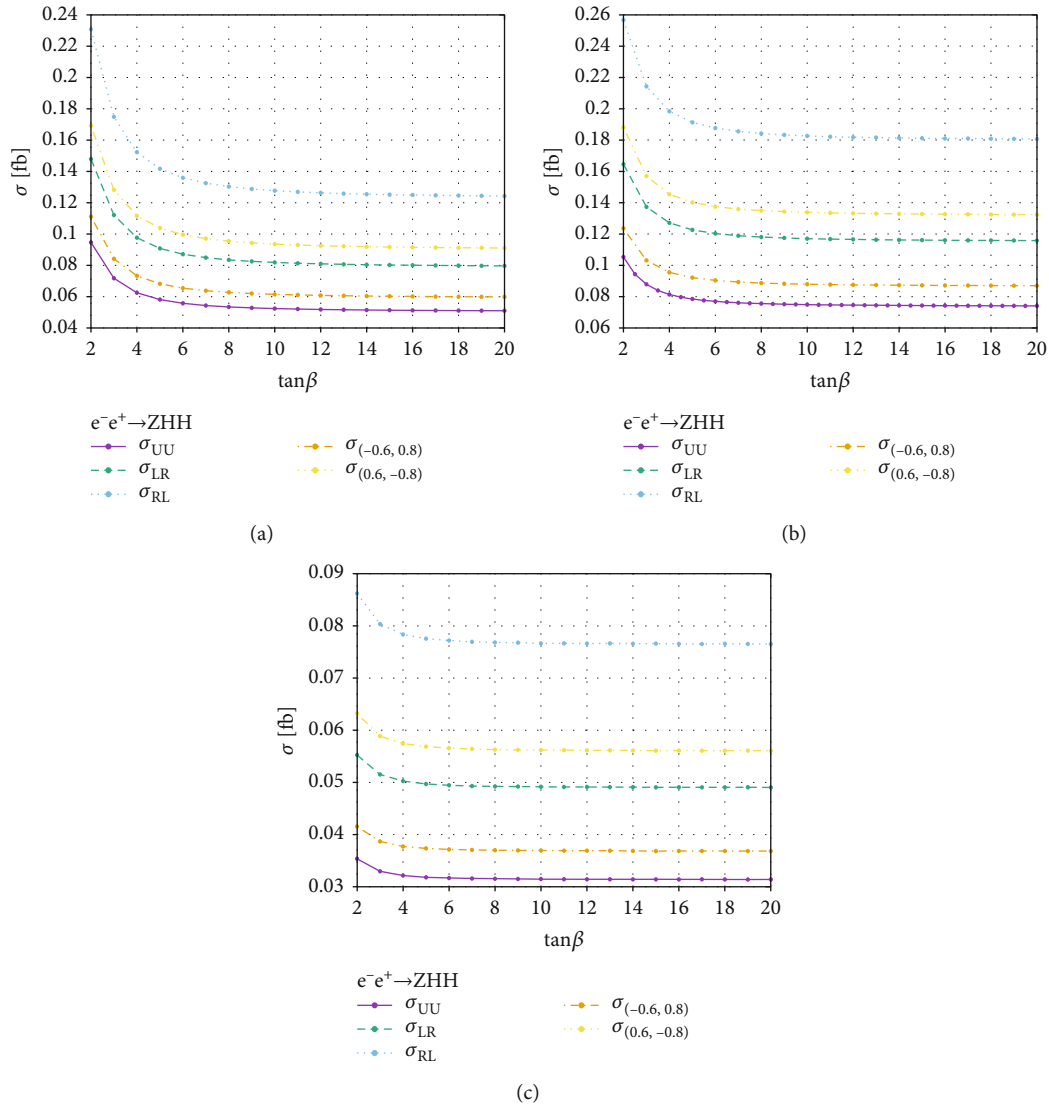

FIGURE 9: In figures, the production cross sections $\sigma(e^+e^- \longrightarrow ZHH)$ are shown as a function of tanβ at (a) 0.6 TeV, (b) 1 TeV, and (c) 3 TeV energies.

In case of $m_H = m_A = m_{H^\pm} = 150$ GeV, the cross-section of unpolarized beam is around $0.0042\,fb$ at 1 TeV which drops rapidly with increase in energy.

6. Dependance of tan β, $\sqrt{s}$, and m_H on the Production Cross-Section

The collisions between electrons and positrons predict the processes without large uncertainties, and the total event rates and shapes are easily manageable. Such colliders have zero charge, zero lepton number, so that it is suitable to create new particles after e^+e^- annihilation. Also, the laboratory frame is the same as the center of mass frame, so that the total center of mass energy is fully exploited to reach the highest possible physics threshold. In e^+e^- collisions, the production cross-section scales asymptotically as $1/s$, like the s-channel processes typically do. This is even true for scattering with t, u-channel diagrams at finite scattering angles. The only exceptions are the processes induced by collinear radiations of gauge bosons off fermions, where the total cross section receives a logarithmic enhancement over the fermion energy. So once the threshold center of mass energy required to produce the desired process is achieved, the maximum production cross-section is obtained and then starts decreasing afterwards. With lepton beams, high degrees of beam polarizations and other asymmetries can be effectively explored.

The variation of production cross-section for all processes, with change in tan β at $\sqrt{s} = 1$TeV, is shown in Figure 17. It can be seen that for the process Zhh, production cross-section remains constant for the two mass values. The reason being the fact that the coupling $g_{h^0h^0h^0}$ for this process is the same as SM one. In the exact alignment limit, the production cross-section for processes ZHH and ZAA have the same distribution because both processes are a function of the same factors as given in Equations (7) and (8). Next, the production cross-section of the processes AHH and AHh is maximum at the low value of tan β and

Table 5: A detailed scan of most relevant parameters of 5 different production processes at Higgs mass $m_\phi = 150$ GeV is performed. At different configuration of beam polarization, the cross-section of selected Higgs production values is obtained.

	0.6 TeV				1 TeV				3 TeV			
	$\tan\beta = 5$	$\tan\beta = 10$	$\tan\beta = 15$	$\tan\beta = 20$	$\tan\beta = 5$	$\tan\beta = 10$	$\tan\beta = 15$	$\tan\beta = 20$	$\tan\beta = 5$	$\tan\beta = 10$	$\tan\beta = 15$	$\tan\beta = 20$
					$e^-e^+ \longrightarrow Zhh$							
σ_UU	0.1869	0.1863	0.1864	0.186	0.1319	0.1316	0.1317	0.1317	0.036253	0.0361733	0.03616	0.0362
σ_LR	029203	0.29120	0.29126	0.29130	0.20615	0.20572	0.20573	0.20573	0.056621	0.056543	0.056539	0.056557
σ_RL	0.45565	0.45426	0.45435	0.45442	0.31259	0.32089	0.32096	0.32098	0.088306	0.088241	0.088241	0.088193
$\sigma\_((0.6,-0.8))$	0.33387	0.33297	0.33301	0.33299	0.23570	0.23521	0.23530	0.23525	0.064696	0.064651	0.064676	0.064674
$\sigma\_((-0.6,0.8))$	0.21934	0.21877	0.21878	0.21880	0.15479	0.15452	0.15454	0.15455	0.042510	0.042491	0.042457	0.042514
					$e^-e^+ \longrightarrow AHh$							
σ_{UU}	0.017277	0.01045	0.00093411	0.0089632	0.013257	0.0077706	0.0068967	0.0065998	0.0021479	0.001047	0.001047	0.00099589
σ_{LR}	0.015155	0.0091414	0.0081716	0.0078409	0.020702	0.01214	0.010770	0.010317	0.0033532	0.0018687	0.0016357	0.0015611
σ_{RL}	0.023581	0.014264	0.012748	0.012232	0.032320	0.018947	0.016800	0.016090	0.0052484	0.0029070	0.0025522	0.0024360
$\sigma_{(0.6,-0.8)}$	0.017277	0.010454	0.0093411	0.0089632	0.023686	0.013889	0.012320	0.011787	0.0038544	0.0021296	0.0018715	0.0017796
$\sigma_{(-0.6,0.8)}$	0.011354	0.0068721	0.0061365	0.0058895	0.015560	0.0091174	0.0080898	0.0077460	0.0025196	0.0014044	0.0012263	0.0011680
					$e^-e^+ \longrightarrow AHH$							
σ_{UU}	0.0067367	0.001894	0.0008613	0.00048807	0.014793	0.0064978	0.0018905	0.001071	0.00321	0.00090088	0.00041045	0.00023214
σ_{LR}	0.010523	0.0029595	0.0013454	0.00076264	0.023111	0.0064978	0.0029554	0.0016753	0.0050175	0.0014085	0.00063930	0.00036364
σ_{RL}	0.016417	0.0046182	0.0020992	0.001897	0.036058	0.010142	0.0046089	0.0026143	0.0078280	0.0022009	0.0010019	0.00056732
$\sigma_{(0.6,-0.8)}$	0.012032	0.0033842	0.0015387	0.00087216	0.026419	0.0074374	0.0033764	0.0019149	0.0057319	0.0016118	0.00073268	0.00041471
$\sigma_{(-0.6,0.8)}$	0.0079058	0.0022240	0.0010107	0.00057310	0.017364	0.0048834	0.0022192	0.0012581	0.0037654	0.0010560	0.00048088	0.00027258
					$e^-e^+ \longrightarrow ZHH$							
σ_{UU}	0.058131	0.052392	0.051358	0.050993	0.078495	0.074928	0.07438	0.07412	0.031811	0.03148	0.031411	0.031407
σ_{LR}	0.090831	0.0818630	0.080237	0.079662	0.12264	0.11703	0.11611	0.11579	0.049703	0.049168	0.049067	0.049034
σ_{RL}	0.14170	0.12771	0.12517	0.1247	0.19129	0.18261	0.18117	0.18065	0.077557	0.076655	0.076611	0.076518
$\sigma_{(0.6,-0.8)}$	0.10384	0.093580	0.091721	0.091077	0.14022	0.13385	0.13275	0.13237	0.056871	0.056211	0.056085	0.056052
$\sigma_{(-0.6,0.8)}$	0.068235	0.061480	0.060274	0.059846	0.092134	0.087936	0.087239	0.086994	0.037366	0.036951	0.036839	0.036841
					$e^-e^+ \longrightarrow ZAA$							
σ_{UU}	0.054229	0.05272	0.052419	0.052313	0.075971	0.075097	0.074993	0.074924	0.031578	0.031489	0.031469	0.031467
σ_{LR}	0.084719	0.08235	0.081905	0.081737	0.11868	0.11735	0.11712	0.11702	0.049323	0.049201	0.049158	0.049131
σ_{RL}	0.13219	0.12851	0.12777	0.12751	0.18521	0.18306	0.18277	0.18261	0.076973	0.076717	0.76681	0.076691
$\sigma_{(0.6,-0.8)}$	0.096858	0.094178	0.093642	0.093460	0.13569	0.13418	0.13389	0.13384	0.056379	0.056242	0.056228	0.056194
$\sigma_{(-0.6,0.8)}$	0.063644	0.061869	0.061510	0.061416	0.089156	0.088173	0.087995	0.087925	0.037060	0.036940	0.036912	0.036923

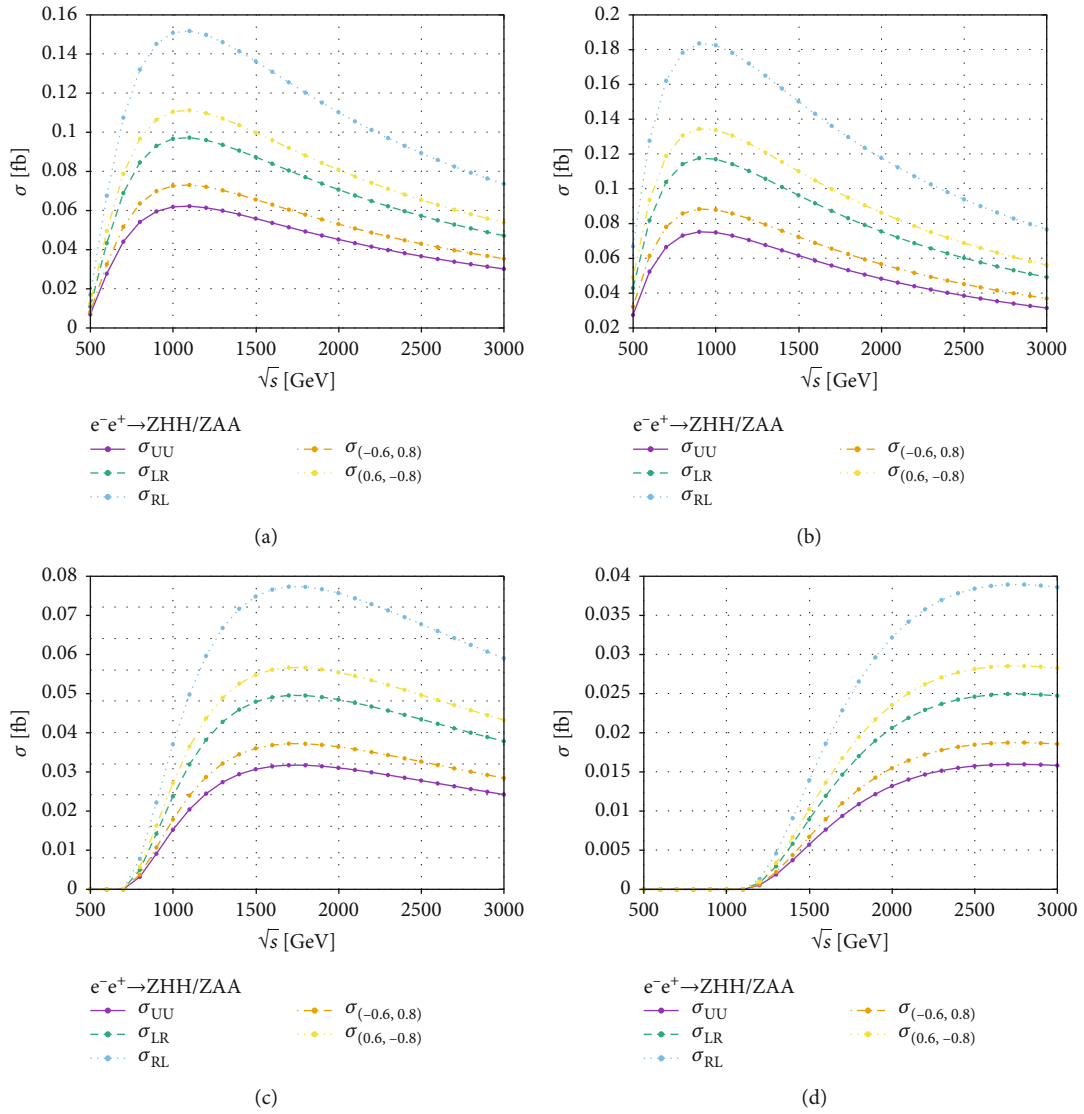

FIGURE 10: Total production cross-section σ (fb) as a function of $\sqrt{s}$ (GeV) is shown in these figures. Higgs mass values $m_{\phi} = 150$ GeV, 175 GeV, 300 GeV, and 500 GeV at $\tan\beta = 10$ and $s_{\beta\alpha} = 1$ are used in figures (a), (b), (c), and (d), respectively.

decrease at higher values of $\tan\beta$ as in type 1 the Yukawa coupling goes inversely proportional to $\tan\beta$.

The distribution of cross-section as a function of m_H is shown in Figure 18. It can be seen that the cross-section for all processes decreases with increasing values of m_H. This is as expected because when the mass of all the extra Higgs states is increased, the phase space becomes narrow for particles in the final state. The process Zhh is an exception, for which the production cross-section remains constant and does not change with a change in the value of m_H.

7. Identifying the Processes

In this section, possible decays of neutral Higgs boson are discussed, and possible colliders for analyzing each of the processes are perceived. The expected number of events and some possible background channels are also discussed.

7.1. Decays of Neutral Higgs Bosons. The branching ratios and decay widths for neutral Higgs Bosons are calculated, whose parameters are explained in Table 6. The branching ratios for Higgs particles H^0, h^0, and A^0 are given as a pie chart. Decay width is defined as the probability of occurance of a specific decay process within a given amount of time. The calculation involves determination of the decay width of neutral Higgs boson based on masses of particles involved and their relevant vertices. While the branching ratio of each Higgs boson remains stable. Further, the decay channels for each of the Higgs bosons remain the same whereas the Higgs mass m_H is changed.

From Figure 19, it is clear that the prominent decay channel for all the neutral Higgs bosons is through b-quarks pair. The branching ratio for $h^0 \longrightarrow b\bar{b}$ is 62%. Similarly, the branching ratios for $H^0 \longrightarrow b\bar{b}$ and $A^0 \longrightarrow b\bar{b}$ are 72% and 54%, respectively. The other possible decay channels for h^0, H^0, and A^0 are gg and cc pairs. It is logical to

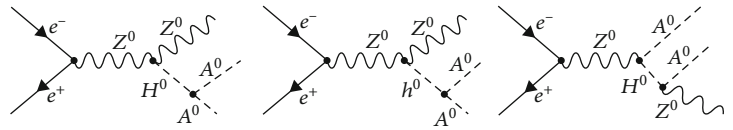

FIGURE 11: Feynman diagrams contributing to the scattering process $e^-e^+ \longrightarrow$ ZAA.

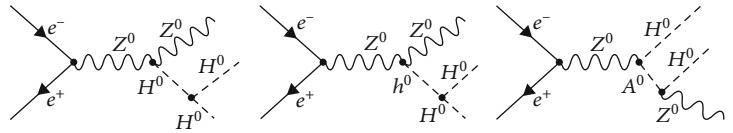

FIGURE 12: Feynman diagrams contributing to the scattering process $e^-e^+ \longrightarrow$ ZHH at ILC.

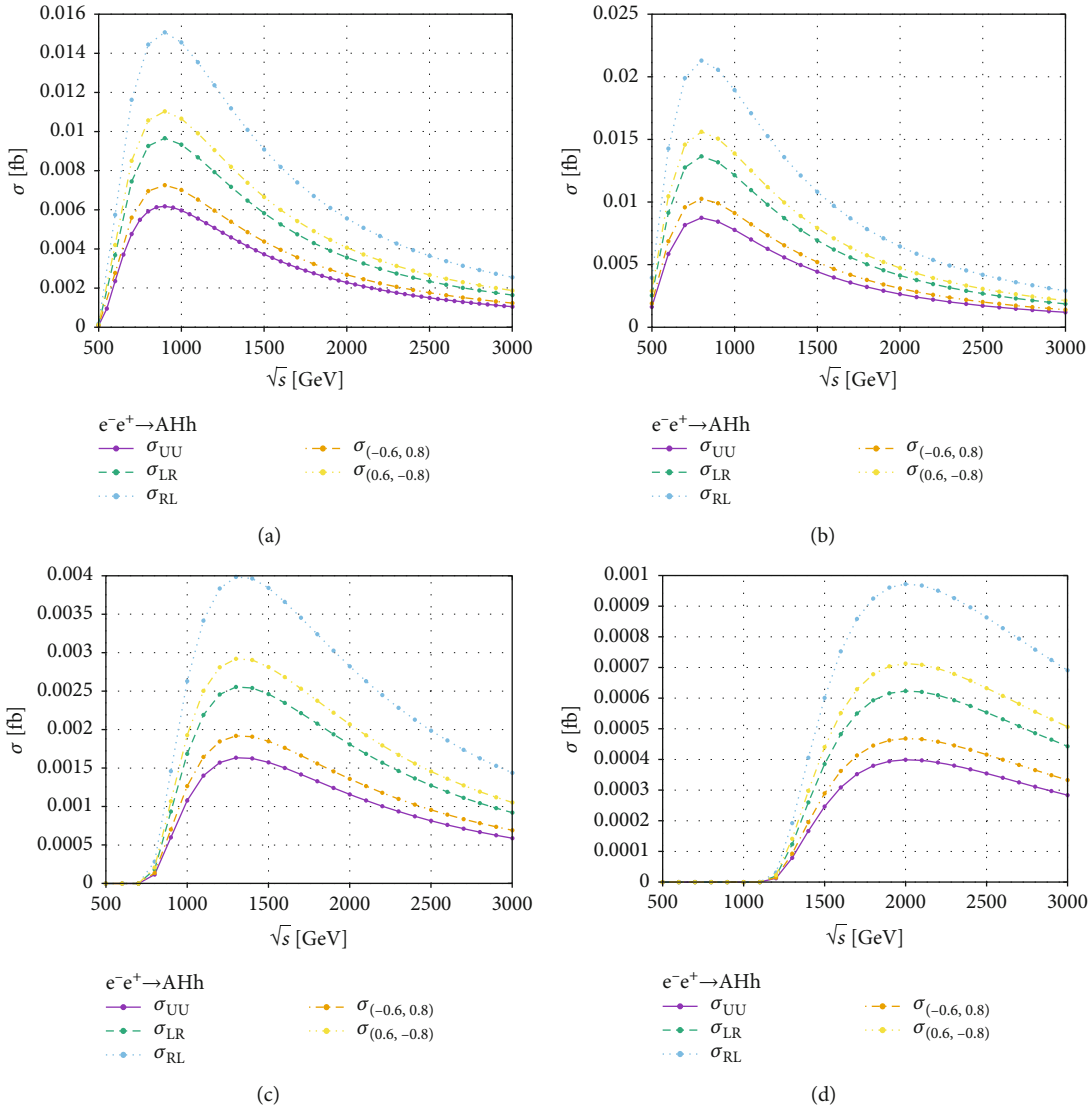

FIGURE 13: The distribution of cross-section σ (fb) as a function of $\sqrt{s}$ (GeV) is ploted in all these plots. Higgs mass values $m_\phi = 150$ GeV, 175 GeV, 300 GeV, and 500 GeV at $\tan\beta = 10$ and $s_{\beta\alpha} = 1$ are used in figures (a), (b), (c), and (d), respectively.

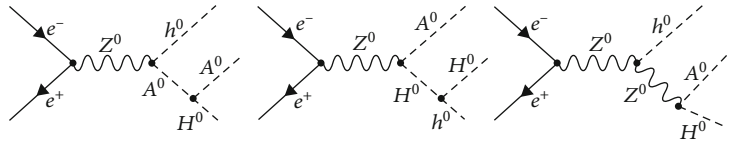

Figure 14: Feynman diagrams contributing to the scattering process $e^-e^+ \longrightarrow ZHH$.

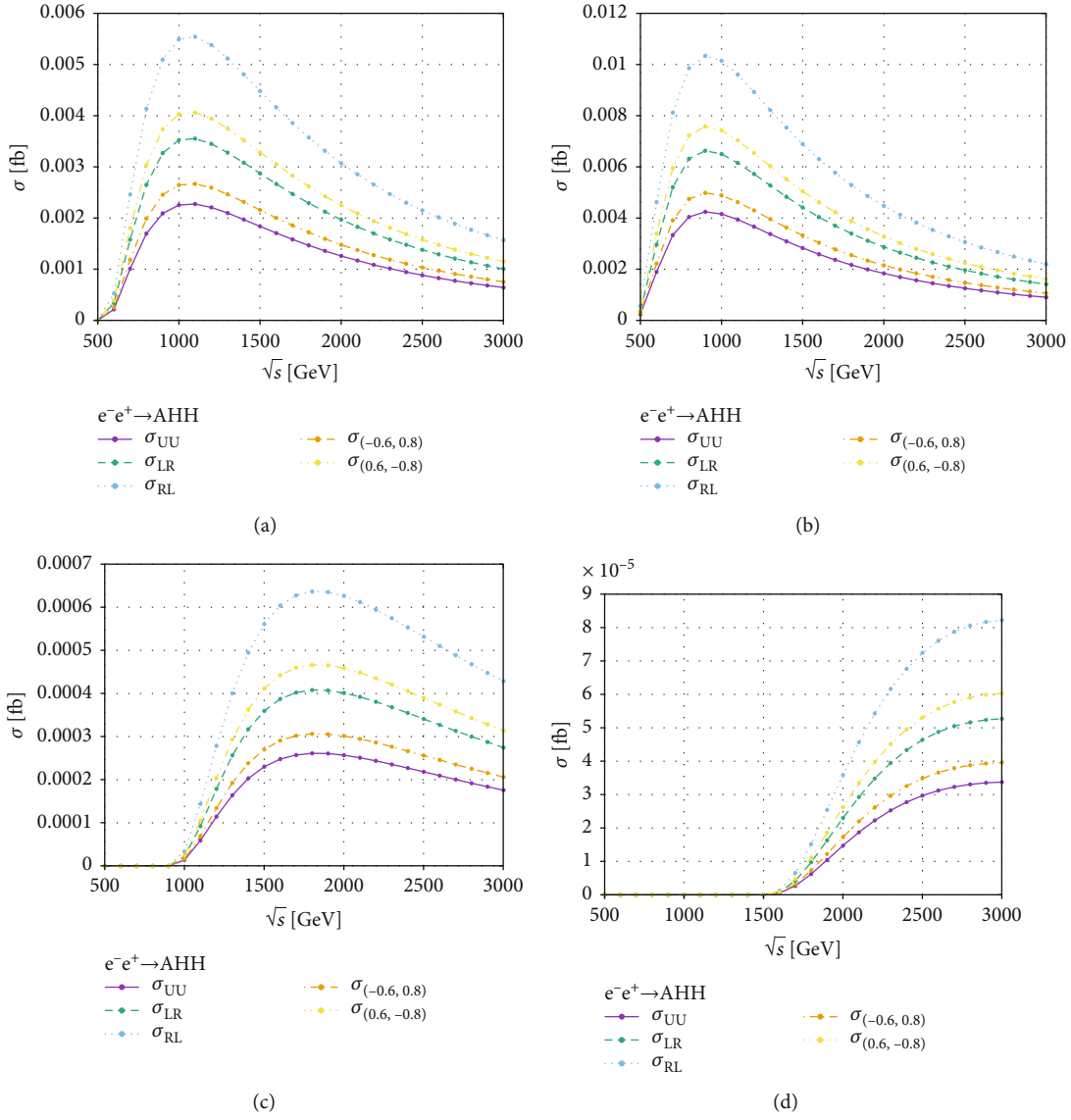

Figure 15: The distribution of cross-section $\sigma\ (fb)$ as a function of $\sqrt{s}$ (GeV) in 2HDM is displayed in above figures, while the Higgs mass values $m_\phi = 150$ GeV, 175 GeV, 300 GeV, and 500 GeV at $\tan\beta = 10$ and $s_{\beta\alpha} = 1$ are taken in figures (a), (b), (c), and (d), respectively.

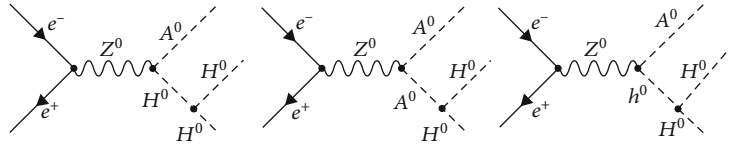

Figure 16: The Feynman diagram for scattering process $e^-e^+ \longrightarrow$ AHH.

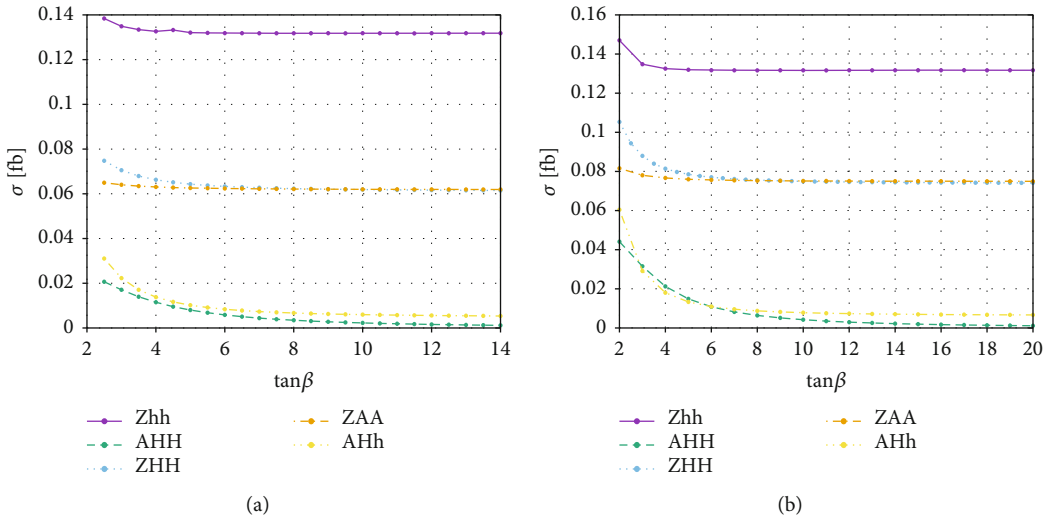

FIGURE 17: Cross-section distribution as a function of tan β for all the processes at $\sqrt{s} = 1$ TeV. The values used are $m_H = 175$ GeV (a) and $m_H = 150$ GeV (b).

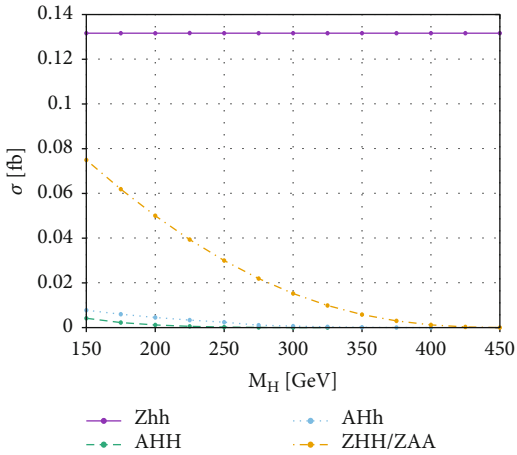

FIGURE 18: The distribution of cross-section as a function of tanβ at $\sqrt{s} = 1$ TeV, where $s_{\beta\alpha} = 1$ and $m_\phi = 150$ GeV.

say that, due to b-quark, gluon, and c-quark pairs, the prominent pattern for each neutral Higgs boson is the di-jet final state in the detector. The next common decay channel is the $\tau\tau$. But the branching ratio of this process is small as compared to the di-jet signal. The h^0 also has other decay channels, which is through W^+W^- and ZZ pair. Hence, these decay channels can be considered as favorable but problem can arise due to leptonic decays of W-boson and extra Z -boson in the final state. Therefore, the hadronic decay channels of h^0 boson promise more in the extraction of its pattern.

7.2. Identification of Processes and Background Channels. In the previous section, decay channels of neutral Higgs boson are discussed and so acquiring the detector pattern of each channel is quite easy. The Z boson decays through a hadronic, leptonic, and invisible channel. The branching ratios of Z boson are $Z \longrightarrow q\bar{q}$ (~ 0.70), $Z \longrightarrow l\bar{l}$ (~ 0.10), and invisible (~ 0.20), respectively. Hence, there will be 4 b -quark jets +2 light jets (coming from Z boson decay) in the final states. Unfortunately, the branching ratio of leptonic decay is small in comparison to the hadronic branching ratio, and there could be fewer events collected in the detector. Some possible patterns at the detectors, percentage of events, and expected number of events are given in Tables 6 and 7 for integrated luminosity values of $1ab^{-1}$ and $3fb^{-1}$. The branching ratio of W and Z are taken from Particle Data Group (PDG) [57], while the branching ratio of all Higgs decaying into bottom quark pair are calculated by Two Higgs Doublet Model Calculator (2HDMC) [27].

It is assumed that International Linear Collider can achieve a total integrated luminosity of $1ab^{-1}$ and $3ab^{-1}$ in its lifetime. The number of events that are expected for various processes in that case are given in Table 7 at $\sqrt{s} = 1$ TeV. Where the $m_H = 175$ GeV and tan $\beta = 10$ are used. Unfortunately, some events for scattering process $A^0H^0h^0$ and $A^0H^0H^0$ are ≤10 and ≤ 6 with $3ab^{-1}$. The number of events could be increased by using polarized incoming beams. However, only this may not give enough cross-section to be useful for the measurement of these two processes. There is some background signal which can hide the actual processes. In SM, the most relevant and expected background channels are $e^+e^- \longrightarrow Zb\bar{b}b\bar{b}$, $e^+e^- \longrightarrow Zcccc$, and $e^+e^- \longrightarrow ZZ \longrightarrow b\bar{b}b\bar{b}$. Hence, reconstruction of the Higgs mass in each event could be beneficial. If neutral Higgs does not decay through $b\bar{b}$ pairs, then, such b-quarks pair will give an invariant mass value that lies outside of the Higgs mass range and such events can be excluded. If the efficiency of b-tagging is measured around 80% or higher, and we require $H_iH_j \longrightarrow b\bar{b}b\bar{b}$ + hadronic decay, this offers a definite pattern at the detector which is 4 b-tagged jets +2 light jets. A notable amount of events can be obtained from this pattern, whereas a big fraction of the background signal could be eliminated, because of b-tagged jet requirements. A Monte

Table 6: The percentage of events for different decay channels is computed by evaluating the branching ratios of each decay mode.

Detector pattern	$Z^0A^0A^0$	$Z^0H^0H^0$	$Z^0h^0h^0$	$Z^0H^0h^0$	$Z^0H^0H^0$
4b-quarks jets+2jets	20.41	36.28	26.91	28.31	35.76
6 jets	60	58	37.30	62	78.71

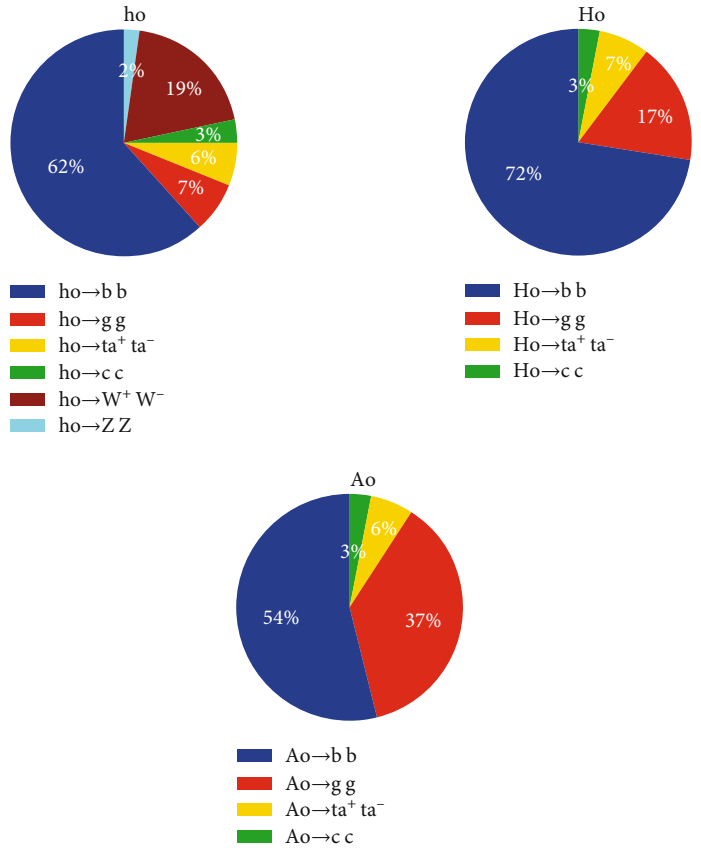

Figure 19: The branching ratios of all neutral Higgs boson decays for parameters defined in Table 6.

Table 7: Expected number of events calculated at different integrated luminosities, $1ab^{-1}$ and $3ab^{-1}$.

Detector pattern	$Z^0A^0A^0$		$Z^0H^0H^0$		$Z^0h^0h^0$		$Z^0H^0h^0$		$Z^0H^0H^0$	
	$1ab^{-1}$	$3ab^{-1}$	$1ab^{-1}$	$3ab^{-1}$	$1ab^{-1}$	$3ab^{-1}$	$1ab^{-1}$	$3ab^{-1}$	$1ab^{-1}$	$3ab^{-1}$
4 b-quarks jets+2 jets	12	39	22	66	35	105	2	4	0.8	2.4
6 jets	38	114	37	111	48	144	3	9	1.7	5.1

Carlo simulation of each of the processes is required to evaluate trigger efficiency and acceptance of the detector for different decay channels.

8. Conclusion

In this study, the production cross-section of various scattering processes is calculated in e^+e^- collider. The scattering process selected to determine the triple Higgs-self coupling is governed by 2HDM. The 2HDM is examined by considering experimental constraints on charged Higgs boson. These constraints probe the exact alignment limit $s_{\beta\alpha} = 1$. There are eight possible Higgs self-couplings, two out of which, the ones for charged Higgs, are not discussed in this study. Due to exact alignment limit $s_{\beta\alpha} = 1$, one of the Higgs self-coupling $g_{h^0h^0H^0}$ vanishes, therefore, only five Higgs self-coupling survive out of eight. The coupling could be determined using the process $Z^0h^0h^0$ which is the same as in Standard Model. The final state of the process $Z^0A^0A^0$ and $Z^0H^0H^0$ helps in extraction of coupling $g_{h^0A^0A^0}$ and $g_{h^0H^0H^0}$. These processes have an acceptable cross-section. Similarly, the coupling $g_{H^0A^0A^0}$ is obtained by the process

$e^+e^- \longrightarrow A^0h^0h^0$. But the cross-section is in attobarn and might not be enough for accumulation of sufficient number of events. At last, the process $e^+e^- \longrightarrow A^0H^0H^0$ extracts the Higgs self-coupling $g_{H^0H^0H^0}$ with the help of $g_{H^0A^0A^0}$, but only if it could ever possibly be determined through the process $A^0H^0H^0$. Although examining the previous process could be difficult, calculating the coupling $g_{H^0H^0H^0}$ is also a challenge using $A^0H^0H^0$ process. The calculation of production cross-section for all the above scattering processes, both with and without polarized beams, shows that the incoming polarized beam enhances the cross-section. The right-handed electron beam and left-handed positron beam enhanced the cross-section up to a factor of 2.4 for all processes. The calculation is carried out in exact alignment limit $s_{\beta\alpha} = 1$ and $m_H = 175\,\text{GeV}$, and $m_H = 150\,\text{GeV}$. The calculation shows that the cross-section increases when $m_H = 150$ GeV is used in comparison to 175 GeV, for all processes, except $Z^0h^0h^0$. The decay widths (not given) and branching ratios of neutral Higgs bosons are also calculated. The study shows that all neutral Higgs bosons have identical decay channels for the specific choice of parameters. The dominant decay channel of all neutral Higgs bosons is through $b\bar{b}$ pair, gluon pair, $c\bar{c}$ pair, and with a small fraction of $\tau\bar{\tau}$. For the measurement of cross-section distribution, ILC has the biggest potential for contribution as compared to the proposed all other future lepton colliders. ILC will operate at a center of mass energy ranging up to 1 TeV. The Future Circular Collider can also make measurements and compete for the couplings $g_{h^0h^0h^0}$, $g_{h^0A^0A^0}$, and $g_{h^0H^0H^0}$ by operating at a center of mass energy range up to 0.5 TeV. However, the Circular Electron-Positron Collider has sufficient center of mass energy to investigate the Higgs self-coupling even for a process like ZHH in SM. The invention of the Higgs boson at LHC has established the Higgs mechanism, generating mass to all particles. This was the last piece of SM and further no clue to new physics has been observed as yet. The simplest extension of SM is 2HDM. This study shows the possible measurement of trilinear Higgs-coupling in the future lepton colliders, which plays a vital role in reconstructing Higgs potential.

Data Availability

The results reported in this manuscript are extracted from manually and locally installed Monte Carlo packages. No data from any official webpage or from any experiment is used in our results.

Disclosure

The current submitted version of manusucript is available on arXiv preprints home page https://arxiv.org/pdf/2110.03920.pdf arXiv:2110.03920.

Conflicts of Interest

The authors declare that they have no conflicts of interest.

Acknowledgments

We gratefully acknowledge support from the Simons Foundation and member institutions.

References

[1] G. Aad, T. Abajyan, B. Abbott et al., "Observation of a new particle in the search for the Standard Model Higgs boson with the ATLAS detector at the LHC," *Physics Letters B*, vol. 716, no. 1, pp. 1–29, 2012.

[2] S. Chatrchyan, V. Khachatryan, A. M. Sirunyan et al., "Observation of a new boson at a mass of 125 GeV with the CMS experiment at the LHC," *Physics Letters B*, vol. 716, no. 1, pp. 30–61, 2012.

[3] The TLEP Design Study Working Group, M. Bicer, H. D. Yildiz et al., "First look at the physics case of TLEP," *Journal of High Energy Physics*, vol. 2014, no. 1, 2014.

[4] M. Xiao, J. Gao, D. Wang et al., "Study of CEPC performance with different collision energies and geometric layouts," *Chinese Physics C*, vol. 40, no. 8, article 087001, 2016.

[5] A. Djouadi, J. Lykken, K. M. Y. Okada, M. Oreglia, and S. Yamashita, *International Linear Collider Reference Design Report Volume 2: Physics at the ILC*https://arxiv.org/abs/0709.1893.

[6] A. Arhrib, R. Benbrik, and C. W. Chiang, "Probing triple Higgs couplings of the two Higgs doublet model at a linear collider," *Physical Review D*, vol. 77, no. 11, article 115013, 2008.

[7] G. Ferrera, J. Guasch, D. Lopez-Val, and J. Sola, "Triple Higgs boson production in the linear collider," *Physics Letters B*, vol. 659, no. 1-2, pp. 297–307, 2008.

[8] M. N. Dubinin and A. V. Semenov, "Triple and quartic interactions of Higgs bosons in the two-Higgs-doublet model with CP-violation," *The European Physical Journal C-Particles and Fields*, vol. 28, no. 2, pp. 223–236, 2003.

[9] G. Chalons, A. Djouadi, and J. Quevillon, "The neutral Higgs self-couplings in the (h)MSSM," *Physics Letters B*, vol. 780, pp. 74–80, 2018.

[10] S. Kanemura, Y. Okada, and E. Senaha, "Electroweak baryogenesis and quantum corrections to the triple Higgs boson coupling," *Physics Letters B*, vol. 606, no. 3-4, pp. 361–366, 2005.

[11] G. Ferrera, J. Guasch, D. Lopez-Val, and J. Sola, "Triple Higgs boson production at the ILC within a generic Two-Higgs-Doublet Model," in *Proceedings of 8th International Symposium on Radiative Corrections — PoS(RAD COR 2007)*, Florence, Italy, 2008.

[12] A. Arhrib, R. Benbrik, and C.-W. Chiang, "Probing triple Higgs couplings of the two Higgs doublet model at linear collider," *Physical Review D*, vol. 77, no. 11, 2008.

[13] A. Gutiérrez-Rodríguez, A. Hernández-Ruíz, O. Sampayo, A. Chubykalo, and A. Espinoza-Garrido, "The triple Higgs boson self-coupling at future linear e+e- colliders energies: ILC and CLIC," *Journal of the Physical Society of Japan*, vol. 77, no. 9, article 094101, 2008.

[14] A. Gutiérrez-Rodríguez, M. A. Hernández-Ruíz, and O. A. Sampayo, "Neutral Higgs boson pair-production and trilinear self-couplings in the Mssm at Ilc and Clic energies," *International Journal of Modern Physics A*, vol. 24, no. 28n29, pp. 5299–5318, 2009.

[15] D. López-Val and J. Solà, "Neutral Higgs-pair production at linear colliders within the general two-Higgs-doublet model:

quantum effects and triple Higgs boson self-interactionsvol. 81, no. 3.

[16] S. Homiller and P. Meade, "Measurement of the triple Higgs coupling at a HE-LHC," *Journal of High Energy Physics*, vol. 2019, no. 3, 2019.

[17] F. Arco, S. Heinemeyer, and M. J. Herrero, "Exploring sizable triple Higgs couplings in the 2HDM," *European Physical Journal C: Particles and Fields*, vol. 80, no. 9, 2020.

[18] G. Moortgat-Pick, T. Abe, G. Alexander et al., "Polarized positrons and electrons at the linear collider," *Physics Reports*, vol. 460, no. 4-5, pp. 131–243, 2008.

[19] G. Moortgat-Pick and S. Riemann, "Presentation at POSIPOL," LAL, Paris, 2007https://indico.lal.in2p3.fr/event/218/.

[20] L. L. Honorez, E. Nezri, J. F. Oliver, and M. H. Tytgat, "The inert doublet model: an archetype for dark matter," *Journal of cosmology and Astroparticle Physics*, vol. 2007, no. 2, p. 028, 2007.

[21] S. L. Glashow and S. Weinberg, "Natural conservation laws for neutral currents," *Physical Review D*, vol. 15, no. 7, pp. 1958–1965, 1977.

[22] S. Kanemura and K. Yagyu, "Unitarity bound in the most general two Higgs doublet model," *Physics Letters B*, vol. 751, pp. 289–296, 2015.

[23] J. F. Gunion and H. E. Haber, "CP-conserving two-Higgs-doublet model: the approach to the decoupling limit," *Physical Review D*, vol. 67, no. 7, article 075019, 2003.

[24] A. W. El Kaffas, W. Khater, O. M. Ogreid, and P. Osland, "Consistency of the two-Higgs-doublet model and CP violation in top production at the LHC," *Nuclear Physics B*, vol. 775, no. 1-2, pp. 45–77, 2007.

[25] N. G. Deshpande and E. Ma, "Pattern of symmetry breaking with two Higgs doublets," *Physical Review D*, vol. 18, no. 7, pp. 2574–2576, 1978.

[26] I. F. Ginzburg and I. P. Ivanov, "Tree-level unitarity constraints in the most general two Higgs doublet model," *Physical Review D*, vol. 72, no. 11, article 115010, 2005.

[27] D. Eriksson, J. Rathsman, and O. Stal, "2HDMC - two-Higgs-doublet model calculator," *Computer Physics Communications*, vol. 181, no. 1, pp. 189–205, 2010.

[28] P. Bechtle, O. Brein, S. Heinemeyer, G. Weiglein, and K. E. Williams, "HiggsBounds: confronting arbitrary Higgs sectors with exclusion bounds from LEP and the Tevatron," *Computer Physics Communications*, vol. 181, no. 1, pp. 138–167, 2010.

[29] P. Bechtle, S. Heinemeyer, O. Stål, T. Stefaniak, and G. Weiglein, "HiggsSignals: confronting arbitrary Higgs sectors with measurements at the Tevatron and the LHC," *The European Physical Journal C*, vol. 74, no. 2, 2014.

[30] T. Enomoto and R. Watanabe, "Flavor constraints on the two Higgs doublet models of Z 2 symmetric and aligned types," *Journal of High Energy Physics*, vol. 2016, no. 5, 2016.

[31] A. Djouadi, H. E. Haber, and P. M. Zerwas, "Multiple production of MSSM neutral Higgs bosons at high-energy e^+ e^- colliders," *Physics Letters B*, vol. 375, no. 1-4, pp. 203–212, 1996.

[32] A. Djouadi, W. Kilian, M. M. Muhlleitner, and P. M. Zerwas, "Testing Higgs self-couplings at e^+e^- linear colliders," *The European Physical Journal C*, vol. 10, no. 1, pp. 27–43, 1999.

[33] P. Oslan and P. N. Pandita, "Measuring the trilinear couplings of MSSM neutral Higgs bosons at high-energye+e−colliders," *Physical Review D*, vol. 59, no. 5, article 055013, 1999.

[34] F. Boudjema and A. Semenov, "Measurements of the supersymmetric Higgs self-couplings and the reconstruction of the Higgs potential," *Physical Review D*, vol. 66, no. 9, 2002.

[35] A. Djouadi, "The search for Higgs particles at high-energy colliders: past, present and future," *Pramana*, vol. 60, no. 2, pp. 215–238, 2003.

[36] A. Djouadi, "The anatomy of electroweak symmetry breaking: Tome I: the Higgs boson in the Standard Model," *Physics Reports*, vol. 457, no. 1-4, pp. 1–216, 2008.

[37] G. Gounaris, D. Schildknecht, and F. Renard, "Test of Higgs boson nature in e+e−→HHZ," *Physics Letters B*, vol. 83, no. 2, pp. 191–194, 1979.

[38] V. Barger, T. Han, and R. J. N. Phillips, "Double Higgs-boson bremsstrahlung fromWandZbosons at supercolliders," *Physics Review D*, vol. 38, no. 9, pp. 2766–2769, 1988.

[39] J. Kamoshita, Y. Okada, M. Tanaka, and I. Watanabe, "Studying the Higgs potential via $e^+e^-$to Zhh," https://arxiv.org/abs/hep-ph/9602224.

[40] D. J. Miller and S. Moretti, "The triple Higgs self-coupling at future e+e- colliders: a signal-to-background study for the standard model," https://arxiv.org/abs/hep-ph/0001194.

[41] D. J. Miller and S. Moretti, "Can the trilinear Higgs self-coupling be measured at future linear colliders?," *The European Physical Journal C*, vol. 13, no. 3, pp. 459–470, 2000.

[42] Y. Yasui, S. Kanemura, S. Kiyoura et al., "Measurement of the Higgs self-coupling at JLC," https://arxiv.org/abs/hep-ph/0211047.

[43] M. Battaglia, E. Boos, and W. Yao, "Studying the Higgs potential at the e+e- linear collider," https://arxiv.org/abs/hep-ph/0111276.

[44] V. Barger and T. Han, "Double Higgs boson production via Ww fusion in Tev E+E−collisions," *Modern Physics Letters A*, vol. 5, no. 9, pp. 667–674, 1990.

[45] A. Dobrovolskaya and V. Novikov, "On heavy Higgs boson production," *Zeitschrift für Physik C Particles and Fields*, vol. 52, no. 3, pp. 427–436, 1991.

[46] D. A. Dicus, K. J. Kallianpur, and S. S. D. Willenbrock, "Higgs boson pair production in the effective-W approximation," *Physics Letters B*, vol. 200, no. 1-2, pp. 187–192, 1988.

[47] A. Abbasabadi, W. W. Repko, D. A. Dicus, and R. Vega, "Comparison of exact and effective-gauge-boson calculations for gauge-boson fusion processes," *Physical review and Physical review letters index*, vol. 38, no. 9, pp. 2770–2775, 1988.

[48] E. W. N. Glover and J. J. van der Bij, "Higgs boson pair production via gluon fusion," *Nuclear Physics B*, vol. 309, no. 2, pp. 282–294, 1988.

[49] T. Plehn, M. Spira, and P. M. Zerwas, "Pair production of neutral Higgs particles in gluon-gluon collisions," *Nuclear Physics B*, vol. 479, no. 1-2, pp. 46–64, 1996.

[50] T. Plehn, M. Spira, and P. M. Zerwas, "Erratum to "Pair production of neutral Higgs particles in gluon-gluon collisions" [Nucl Phys. B 479 (1996) 46]," *Nuclear Physics B*, vol. 531, no. 1-3, p. 655, 1998.

[51] S. Dawson, S. Dittmaier, and M. Spira, "Neutral Higgs-boson pair production at hadron colliders: QCD corrections," *Physical Review D*, vol. 58, no. 11, article 115012, 1998.

[52] G. Jikia, "Higgs boson pair production in high energy photon-photon collisions," *Nuclear Physics*, vol. 412, no. 1-2, pp. 57–75, 1994.

[53] G. Moortgat-Pick, T. Abe, G. Alexander et al., *Revealing fundamental interactions: the role of polarized positrons and electrons*

at the linear collider (No. SLAC-PUB-11087), Stanford Linear Accelerator Center (United States). Funding organisation: US Department of Energy (United States), 2005.

[54] K. Fujii, C. Grojean, M. E. Peskin et al., "The role of positron polarization for the inital 250 GeV stage of the International Linear Collider," 2018, https://arxiv.org/abs/1801.02840.

[55] A. Belyaev, N. D. Christensen, and A. Pukhov, "CalcHEP 3.4 for collider physics within and beyond the Standard Model," *Computer Physics Communications*, vol. 184, no. 7, pp. 1729–1769, 2013.

[56] S. Eidelman, K. G. Hayes, K. E. Olive et al., "Review of particle physics," *Physics Letters B*, vol. 592, no. 1-4, pp. 1–5, 2004.

[57] P. A. Zyla, R. M. Barnett, and J. Beringer, "Particle Data Group," *Progress of Theoretical and Experimental Physics*, vol. 2020, article 083C01, 2020.